Investigation of the performance of a hybrid wind turbine Darrieus-Savonius

UNIVERSITY OF RUSE "ANGEL KANCHEV"

AGRARIAN AND INDUSTRIAL FACULTY
Department of Thermotechnics, Hydraulics and Ecology

MSc. Eng. Ahmed Syuleymanov Ahmedov

Investigation of the Performance of a Hybrid Wind Turbine Darrieus-Savonius

ABSTRACT

of a PhD Thesis for the Educational and Scientific Degree
"DOCTOR"

Doctoral programme:
Hydraulic and Pneumatic Machines and Equipment

Scientific Supervisors:

Assoc. Prof. Krasimir Ivanov Tujarov, PhD
Prof. Gencho Stoykov Popov, PhD

Reviewers:

Prof. Gancho Varbanov Guzhgulov, PhD

Assoc. Prof. Todor Ivanov Chakarov, PhD

RUSE, 2016

The PhD thesis was developed by the PhD student during the State Doctoral programme at the department of "Thermotechnics, Hydraulics and Ecology" in University of Ruse "Angel Kanchev".

The experimental investigations regarding the PhD thesis had been conducted at the "Fluid Mechanics and Hydraulic and Pneumatic Equipment and Machinery" laboratory of University of Ruse "Angel Kanchev".

The PhD thesis has 5 chapters and it contains 218 pages, 143 figures and 14 tables. A total of 130 references have been cited, 13 of which in Cyrillic and 117 in Latin.

The PhD thesis has been presented and discussed at an expanded faculty council meeting at the department of "Thermotechnics, Hydraulics and Ecology" of University of Ruse "Angel Kanchev" on 07/04/2016. The thesis was approved and forwarded for official final presentation in front of a scientific jury.

The doctoral exam will be carried out in an open session format in front of a scientific jury appointed by the University of Ruse "Angel Kanchev" Rector on 02/06/2016, at 16:00 in room 9.3, building 9. The Doctoral candidate materials will available at the department of "Thermotechnics, Hydraulics and Ecology".

The Abstract of the PhD Thesis is published on the university's website for academic staff development.

Author: MSc. Eng. Ahmed Syuleymanov Ahmedov
Title: "Investigation of the Performance of a Hybrid Wind Turbine Darrieus-Savonius"

OVERALL CHARACTERISTIC OF THE DOCTORAL THESIS

Problem Actuality

The constantly rising fossil fuels prices and the different agreements between the industrialized countries for carbon dioxide emissions reduction are driving forward the renewable energy sector development. The wind energy systems are one of the most popular, cost-effective systems in comparison with most of the available renewable energy utilizing systems to date. Due to this fact, the interest and investments in wind energy systems are steadily growing through the last decade. The investment in the wind energy sector for the European Union member states is expected to reach 20 billion euro until 2030. The need of sustainable "green" households and the new European legislation regarding that problem are contributing to the integration of the wind energy systems into the urban areas. According to the above-pointed facts the wind energy sector stands as a major point of interest for further study, development and innovation.

Doctoral Thesis Objective and Tasks

Objective: Investigation of the force interaction between an air flow and a hybrid wind turbine rotor type Darrieus-Savonius. Obtaining the hybrid turbine's performance and aerodynamic characteristics.

The objective of the doctoral thesis is met through the completion of the following set of tasks:

1. Development of a 2D and 3D theoretical computational models for the evaluation of the velocity and pressure fields through the turbines wind rotor. Computing the turbulent flow through the rotor by the aid of appropriate software, using the Reynolds Navier-Stokes partial differential equations.

2. Development a method for rotor's torque and drag force evaluation based on the theoretical analysis results.

3. Development of an experimental investigation methodology for the hybrid wind rotor operation. Conduction of experimental investigations and obtain the rotor's torque and drag forces. Comparing the theoretical and experimental results.

4. Improvement and refinement of the theoretical analysis methodology for a flow passing through a hybrid wind turbine with vertical axis of rotation type Darrieus-Savonius, based on the conducted theoretical and experimental investigations.

Investigation Methods

The adopted main investigation methods regarding the completion of the thesis set of tasks are as follows: creation of a geometrical model (2D and 3D) for all of the turbine's investigated designs; computational mesh generation – finite volume method; computational solver setup, software used ANSYS Fluent 14.0; conduction of a numerical modelling over the force interaction between an air flow and rotating wind rotor; development of an methodology for experimental investigation of vertical axis wind turbines; manufacturing of an multifunctional test bench for experimental analysis of wind turbines; evaluation of the accuracy of the experimental measurements over the turbine performance - torque, drag force, rotational speed, wind speed etc.

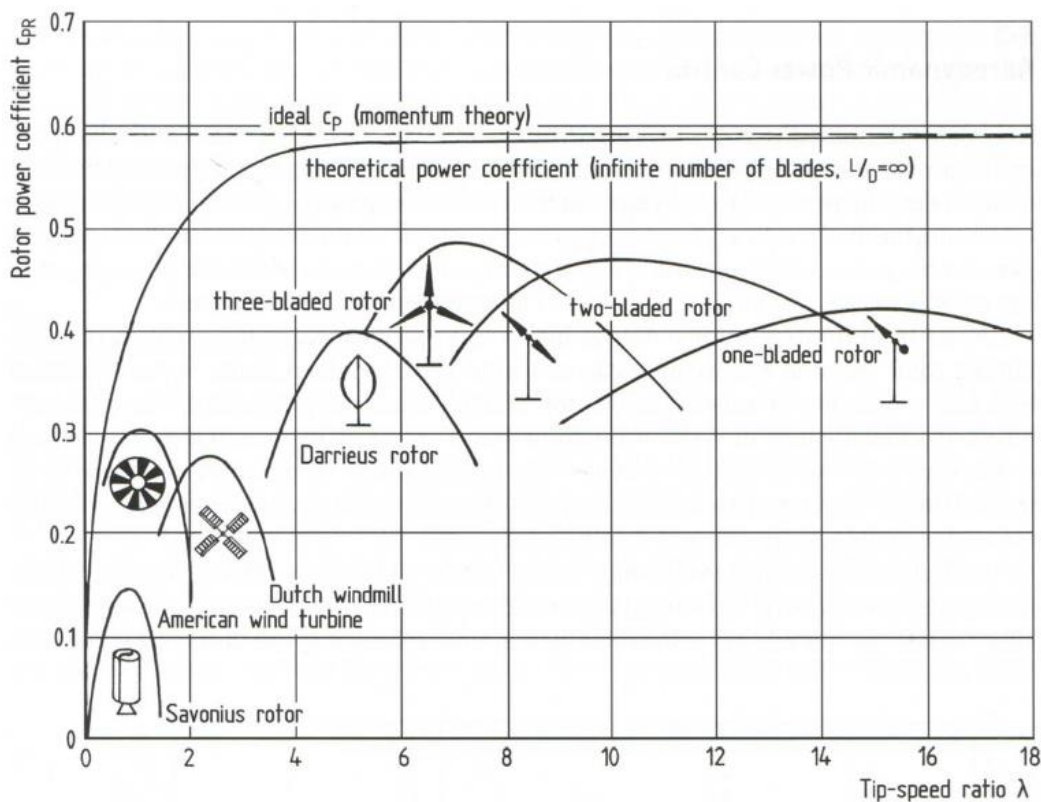### Approbation

A total number of 5 published scientific papers regarding the Doctoral thesis has been presented. One of which is published in the international American Journal of Energy Research, online 2017, the second one is published in the journal of "Mechanic of the machines", Varna 2013, the rest of the papers are published in "University of Ruse Proceedings", Ruse 2012, 2013 and 2014.

CONTENT OF THE DOCTORAL THESIS

1. CHAPTER INTRODUCTION

The constantly rising fossil fuels prices and the different agreements between the industrialized countries for carbon dioxide emissions reduction are driving forward the renewable energy sector development. The wind energy systems are one of the most popular and cost-effective systems in comparison with most of the available renewable energy utilization systems to date. Due to this fact, the interest and investments in wind energy systems are steadily growing through the last decade. The investment in the wind energy sector for the European Union member states is expected to reach 20 billion euro until 2030. The increase of the energy supplied to the electrical grid by wind turbines will affect the stability and quality of the commercial grid. The decentralized electrical energy generation is an important aspect of the development of a unified "intelligent" electrical distribution grid focused on urban application. Furthermore, the need of sustainable "green" households and the new European legislation regarding that problem are contributing to the integration of the wind energy systems in the urban areas. According to the above, the wind energy sector arises as a major point of interest for further study, development and innovation.

Regarding their axis of rotation, the wind turbines can be divided into two major groups – wind turbines with horizontal axis of rotation (HAWT) and wind turbines with vertical axis of rotation (VAWT). The maximum efficiency value of the VAWT is lower in comparison with the HAWT efficiency value. But unlike the HAWT the VAWT has not been an object of intensive research. Typical representatives of the VAWT are the Darrieus and Savonius wind rotors and their hybrid configuration – Darrieus-Savonius.

Fig. 1. Graphical dependency $C_P = f(\lambda)$ for different types wind turbines

The main advantage of the VAWT is that they do not need an additional mechanism for orientation towards the wind direction. This advantage is especially valuable in areas

with frequent changes in the wind direction. The VAWT configuration allows for the electrical generator and mechanical transmission to be mounted on the ground level of the turbine. In that case, the central pylon does not have to carry the weight of the generator and the gearbox. Also, this design allows for easy access to the generator room for service and maintenance operations. The mounting of VAWT on towers is hard to perform. This means that these machines are usually mounted on ground level or on rooftops of different type of buildings. When mounted on rooftop the rooftop affects the wind flow, resulting in increased wind speed (at tall buildings) which benefits the turbine performance. If the turbine height is 50% of the building height on which it is mounted, then the turbine will operate in favourable conditions of lower turbulence and higher wind flow speed.

In the urban areas, the wind flow is highly turbulent with rapidly changing direction and speed. The VAWT perform well in conditions of strong wind gusts. The VAWT can be successfully used in urban and isolated montane areas as an alternative to the conventional HAWT.

Fig. 1 depicts the graphical dependency between the power coefficient C_P and the tip speed ratio (TSR) λ for different types of wind turbines. Even though the HAWT reaches higher power coefficient values in comparison with the VAWT, some of the advantages of the latter have led to increase in their popularity in recent years. It is important to note that no type of wind turbine can reach power coefficient higher than 0.59 (the Betz limit). Therefore, no significant increase in the efficiency of the commercial wind turbines is to be expected. The TSR is a criterion used for evaluation of the turbines noise production. The higher the TSR the noisier the turbines are. Iida et al. prove that the VAWT reaches up to 70dB during operation which is with 10dB lower in contrast with the HAWT.

The consumer and industry interest toward the VAWT due to their advantages impose a deeper investigation of their kinematic, static and dynamic performance characteristics to increase their efficiency and refine their design.

2. CHAPTER ANALYSIS OF THE INVESTIGATED PROBLEM CURRENT STATE

2.1. Analysis of the Theoretical Investigations Over VAWT

The VAWT investigations began during the 70s of the past century. A numerous experimental and theoretical investigations had been conducted. Different types of analytical models were created, and large amounts of experimental data were acquired. In recent years there is a rise in the interest towards the numerical modelling approach - computational fluid dynamics (CFD).

The numerical modelling is divided into two major groups. The first one is expressed through mathematical modelling (analytical models) where the problem is described by the aid of mathematical dependencies. The analytical models allow for the prediction and evaluation of the flow field through the wind rotor and the blade loads. Those models are derived from the fundamental aerodynamic theories.

The second group of theoretical modelling includes the computational fluid dynamics (CFD) approach. At this approach, the whole flow area including the near wall regions (the blades) can be solved through a couple of different forms the Navier-Stokes partial differential equations. The Reynolds Averaged Navier-Stokes (RANS) equations are an example for a concrete form of the governing equations which includes a set of turbulent equations called turbulence models. These turbulence models are bringing the Navier-Stokes differential system to a state in which it can be solved. The fluid area (computational domain) is divided into small volumes (cells). The parameters of the flow are computed for each cell. The CFD approach has the edge over the analytical approach due to the less degree of assumptions and simplifications made regarding the forces acting on the blades.

❖ ***Main Parameters of VAWT***

The main mathematical dependencies which are shared between the aerodynamic models are presented below.

One of the main parameters of the VAWT is the tip speed ratio (TSR) λ. The TSR presents a ratio between the blades peripheral velocity and the wind flow velocity. The TSR is defined as follows:

(1)
$$\lambda = \frac{u}{\vartheta_\infty},$$

Where $u = \omega_{AV}.R$ is the rotor peripheral velocity, R is the rotor radius and ϑ_∞ is the wind flow velocity.

The velocity and force triangles which are defining the flow kinematics and its force interaction with the rotor blades are shown in fig. 2. The velocity of the undisturbed airflow is denoted with ϑ_∞. At wind turbine rotation with angular velocity ω_{AV}, the value of the relative velocity W which is attacking the blade at point M is changing with the blades angular position. Point M lies upon the blade trajectory therefore, it can be written $\overrightarrow{OM} = \overrightarrow{R}$. As can be seen from the figure the relative velocity is action upon the blade surface which is facing the flow. In the upstream area ($270° \le \theta \le 90°$) the relative force is acting upon the suction side of the blade. With the turbine rotation, the blade reaches the downstream area ($90° \le \theta \le 270°$) where W starts to act upon the blade pressure side. During the blade full revolution, the values of the angle of attack are changing in a range from positive to negative. The relative velocity and the angle of attack are determined by the following equations:

(2)
$$W = \vartheta_\infty \sqrt{1 + 2\lambda \sin\theta + \lambda^2},$$

(3)
$$\alpha = arctg\left(\frac{\sin\theta}{\cos\theta + \lambda}\right),$$

where θ is the angular position of the blade regarding the Y-axis. The total output power P of the turbine is calculated through the equation:

(4)
$$P = M\omega_{AV},$$

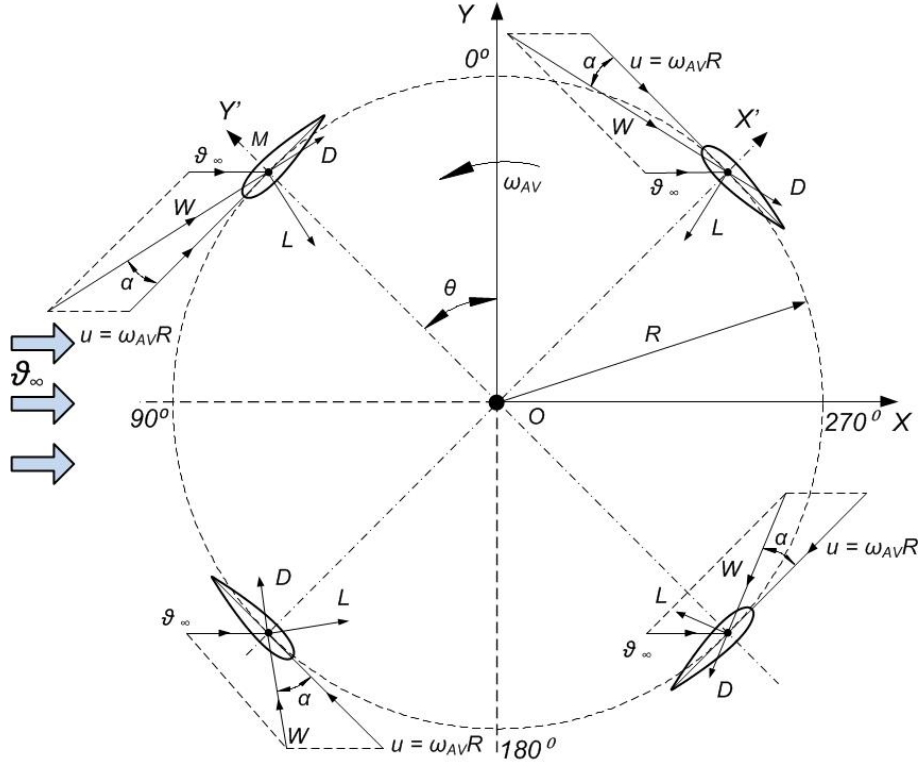where M is the wind rotor torque and ω_{AV} its the angular velocity.

Fig. 2 Velocity and force triangles

❖ *Analytical Performance Investigation Models for VAWT*

The single streamtube, multiple streamtube and double-multiple streamtube models are developed based on the actuator disk theory applied for wind turbines. The first implementation of the actuator theory for wind turbines performance prediction was done by Glauert. According to the actuator disk theory limitations, the streamtube models are applicable only for wind turbines with solidity of $\sigma < 0.2$ operating in narrow range of TSR. Furthermore, the flow is assumed to be quasi-steady and for the evaluation of the blade forces, experimental tabular data regarding the lift force and drag force coefficients are used. All the aforementioned assumptions are compromising the accuracy of the blade forces modelling. The impulse models are not capable of detailed modelling of the flow in the near blade region, the vortex generation and development and the vortex trail behind the wind rotor.

Another typical representative of the analytical models are the vortex models. The vortex models are developed on the assumption for potential, incompressible flow. The vortex models allow for the modelling of the vortex trail behind the rotor. The turbine blades are represented as vortex filaments. The vortex model concept is introduced for the first time by Larsen. The vortex models take more computational time in contrast with the streamtube models. This is due to the Biot-Savart law computation for every detached vortex in the flow field. The vortex models, performance prediction data is more physically realistic in comparison with the impulse models despite the assumption for inviscid flow.

The computational fluid dynamics (CFD) approach implements the Averaged Reynolds Navier-Stokes equations for the VAWT performance prediction. The CFD simulation results give a deeper insight of the operational principals of the VAWT. The ability of the CFD approach to calculate the aerodynamic forces acting on the blades, eliminates the need for experimental tabular data incorporation, regarding the static and dynamic aerodynamic force coefficients. The unsteady operational nature of the VAWT requires highly adaptable modelling approaches such as the RANS and LES (Large Eddy Simulation) CFD models. The RANS approach allows for the calculation only of the main flow, where the turbulent pulsations are modelled by the introduction of additional stress tensors called Reynolds stress tensors. In the case of isotropic turbulence, the Reynolds stress tensors are reduced to scalars which are acting as turbulent viscosity. In this situation, the turbulent viscosity relates to one or several turbulence parameters (turbulent kinetic energy – k and turbulent dissipation - ε) for which semi-empirical dependencies are being calculated. The most popular turbulent models which are incorporating the approach are Spalart-Allmaras (one equation model) and the two-equation models $k-\varepsilon$ and $k-\omega$. The hybrid turbulent model $k-\omega\ SST$ is superior in terms of flow modelling involving vortex generation, separation and interaction. This is due to the combination of the excellent near wall treatment of the $k-\omega$ model and the superior modelling of the main flow provided by the $k-\varepsilon$ model.

More precise CFD modelling approach is the LES (Large Eddy Simulation) approach. This model allows for the direct calculation of the large eddies through the governing equations, while the smaller eddy structures are being modelled. The LES approach is applicable only for 3D simulations. The LES simulations are computationally intensive, they have high demands toward the computational meshes densities and are taking significantly more computational time in comparison with the RANS approach. The main reason for those high demands is the direct calculation of the turbulence parameters for the large eddies through the governing equations.

One of the main challenges before the mathematical modelling of the VAWT operation is the dynamic stall phenomena modelling. It occurs in a wide range of operational regimes. The dynamic stall is characterized by generation and detachment of vortex structures from the suction side of the blades, causing change in the blades angle of attack. If the frequency and the amplitude of change in the angle of attack are sufficiently pronounced a clear pattern of vortex generation and shedding is observed. This phenomenon arises as a steep challenge to the CFD VAWT operation modelling techniques.

The URANS approach in combination with the $k-\omega\ SST$ model can model the pronounced unsteady nature of the flow passing through the rotor of a VAWT. This approach can model the dynamic stall phenomena whit satisfactory accuracy. Despite the LES modelling supremacy over the URANS approach the high computational hardware demand and the long computational time are limiting its application.

2.2 Analysis of the Experimental Investigations of VAWT

The experimental methods for VAWT operation investigation are divided in field tests at which a real size turbine is tested in field conditions and laboratory investigations at which a model turbine is studied in wind tunnels by the aid of specialized test equipment. The laboratory experimental investigations can be further divided into the following three groups:

➢ Experimental methods for VAWT operational performance characteristics derivation.
➢ Experimental methods for analysis of the instantaneous aerodynamic forces acting on the rotor's blades.

➤ Visualization of the flow passing through the turbine rotor.

The approaches for experimental derivation of the performance and aerodynamic VAWT characteristics are providing data regarding the turbine's steady operational regimes. Here of major importance are the time-averaged performance parameters of the investigated turbine. In the case of instantaneous performance parameters analysis, the major setback is that the parameters are continuously changing whit the turbine rotation. Their evaluation requires specialized equipment whit high-frequency writhing speeds and high accuracy class.

The derivation of reliable, repeatable experimental data from the test bench equipment regarding the aerodynamic forces acting on the turbine blades is considered a steep challenge. The aerodynamic loads are measured through openings on the blade surface. By their aid, the pressure distribution along the airfoil profile is obtained. The loads can also be measured with system of load cells placed in the blade-to-strut mounting points.

The experimental evaluation of the instantaneous values of the aerodynamic blade forces is a complex and sophisticated to achieve initiative. This type of dynamic experimental investigations is bound with specific and difficult to implement requirements regarding the test bench design and the measuring equipment properties. On the other hand, the experimental steady operational regimes analysis approach provides sufficiently detailed information for the time-averaged VAWT performance parameters. The development and construction of steady operational regimes analysis experimental methodology and test bench are relatively simple regarding the technical and financial aspects.

2.3. Analysis of the Investigated Problem Current State Conclusions

Based on the conducted literature review the following conclusions are made:

1. In the literature VAWT, analytical prediction models are predominant. The main drawbacks of the analytical models are the assumption for potential flow passing through the rotor and the introduction of the viscosity by empirical coefficients. Most of the analytical models are applicable only for turbines with low solidity operating with high tip speed ratios. Only a small number of turbine designs and limited operational regimes can be investigated through the analytical prediction models.

2. The majority of the VAWT researchers had conducted 2D CFD modelling by implementing the URNS approach. The URANS modelling accuracy of the flow passing through the turbine is relatively compromised. The theoretical results are overestimating the experimental data and the theoretical performance curves are displaced regarding the experimental curves.

3. The theoretical results in the available literature are pointing that the hybrid turbulent model $k - \omega\ SST$ is modelling the aerodynamic performance of the VAWT with satisfactory accuracy. This model is combining the excellent near wall flow treatment of the $k - \omega$ and the superior handling of main flow provided by the $k - \varepsilon$ model.

4. The analysis of the theoretical results provided by the LES and DES approaches is showing that at flows with average to high Reynolds numbers the DES model uses the RANS approach for the near wall flow modelling. In those cases, the flow field around the blades obtained through the DES model is extremely close to the flow obtained by the RANS approach.

5. Most of the CFD simulations of VAWT operation prediction are carried out for either a Savonius type VAWT or Darrieus type VAWT. The most appropriate numerical approach for modelling the performance of a hybrid rotor Darrieus-Savonius is to be determined.

6. The influence of the wind rotor solidity, blades pitch angle and the blades number over the operational and aerodynamical characteristics of the hybrid wind turbine Darrieus-Savonius needs further investigation.

7. The critical value of the Reynolds number Re_{CR} at which the wind rotor starts to operate in fully developed turbulent flow regime needs further investigation.

2.4. Objective and Tasks

Based on the conclusions derived from the literature review analysis the following Objective of the Doctoral thesis is set:

Investigation over the force interaction between an air flow and a hybrid wind turbine rotor type Darrieus-Savonius. Obtaining the hybrid turbine's performance and aerodynamic characteristics.

To meet the set Objective, the following tasks are formed:

1. Development of a 2D and 3D theoretical computational models for the evaluation of the velocity and pressure fields through the turbines wind rotor. Computing the turbulent flow through the rotor by the aid of appropriate software, using the Reynolds Navier-Stokes partial differential equations.

2. Development a method for rotor's torque and drag force evaluation based on the theoretical analysis results.

3. Development of an experimental investigation methodology for the hybrid wind rotor operation. Conduction of experimental investigations and obtain the rotor's torque and drag forces. Comparing the theoretical and experimental results.

4. Improvement and refinement of the theoretical analysis methodology for a flow passing through a hybrid wind turbine with vertical axis of rotation type Darrieus-Savonius, based on the conducted theoretical and experimental investigations.

3. CHAPTER THEORETICAL INVESTIGATIONS

3.1. Theoretical Investigation Prerequisites

The symmetric airfoils are widely used in VAWT constructions due to the abundance of data regarding their aerodynamic characteristics. The available research data shows that airfoils with smaller thickness have weak self-starting capabilities, whereas the airfoils with larger thickness have better self-starting capabilities. On the other hand, the airfoils with larger thickness have greater drag resistance which leads to drop in the turbine power coefficient. It has been established that the airfoils with optimal shapes are the NACA $0020 \div 0025$.

The helical type blade shape contributes to a smoother torque generation during the turbine operation. This ensures longer operational life for the wind rotor. The investigations of different wind rotor shapes (H-shaped, V-shaped, Troposkien-shaped and Helical-shaped) designs shows that the Helical-Shaped rotors are reaching highest power coefficient C_P values.

The advantages of the Helical-Shaped blades are not sufficient to overthrow the straight blade shape rotor designs. The Helical-Shaped blades are difficult to manufacture and significantly more expensive in comparison with the straight blade design. Due to the above-stated reasons, the design of the investigated hybrid wind turbine will incorporate straight bladed rotor design (H-rotor) with symmetric airfoils type NACA 0021.

The vertical axis wind turbine solidity is defined as:

(5)
$$\sigma = \frac{N c L_b}{S} = \frac{N c}{D},$$

where N is the blades number, L_b is the blade length, c is the blade chord length, D is the turbine diameter, $S = D.L$ is the rotor swept area.

If the turbine diameter is a constant geometrical parameter, equation (5) shows that the solidity is affected by the blades number and their chord length. The solidity of the investigated rotor is altered through the change of the blades number. The chord length is kept constant while the blades number is increasing N = 2,4. According to (5) the investigated rotor solidities yield $\sigma = 0.35; 0.7$.
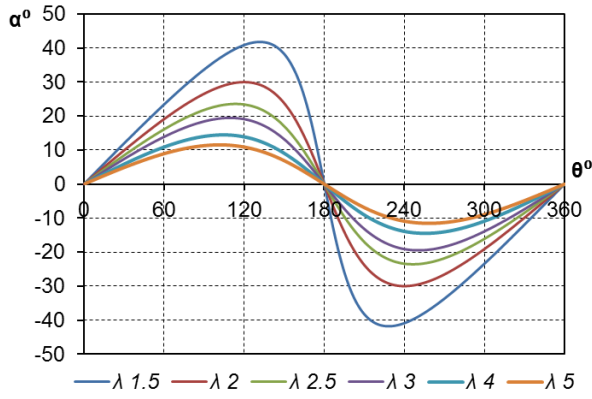
❖ Phenomena Occurring in a Flow Passing Through a Wind Rotor

The reduce frequency k^* presents a ratio between the time for which the flow passes from the blade leading edge to its trailing edge and the time for which the angle of attack changes from its minimum to its maximum values. The reduced frequency Is evaluated by:
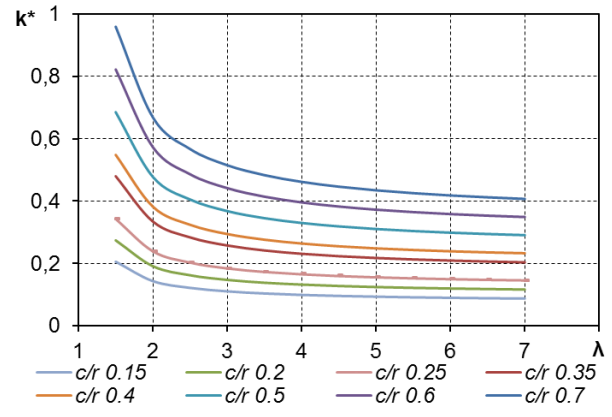
(6)
$$k^* = 0.5 \left(\frac{c}{R} \right) \left(\frac{1}{\lambda - 1} \right) / \arctan\left(1/ \sqrt{\lambda^2 - 1}\right).$$

Fig. 3 depicts the change in the angle of attack as a function of the rotor angular position θ relative to the OY axis at different tip speed ratios (3). The angle of attack values $\alpha \geq 12°$ at which dynamic stall occurs is never reached at TSR $\lambda > 5$. At TSR $\lambda = 5$ a light dynamic stall might occur. At TSR $\lambda = 1.5 - 3$ the angle of attack is changing in the range of $\alpha = \pm 20° \div \pm 40°$ which results in the occurrence of deep dynamic stall phenomenon.

Fig. 4 presents the reduced frequency as a function of the TSR for several different ratios of the blade chord to the rotor radius c/R. If the value of k^* is lower than 0.005, it is assumed that the flow is quasi-steady. As can be seen from the figure, for values of c/R greater than 0.2, k^* values are exceeding 0.05 regardless of the TSR. The flow passing through the investigated turbine is unsteady since $c/R = 0.07/0.2 = 0.35$.

Fig. 3 Angle of Attack as a Function of the Rotor Angular Position

Fig. 4 Reduce Frequency as a Function of the TSR

❖ Nature of the Air Flow Passing Through the Wind Rotor

The balance between an adequate physical CFD modelling of the rotor blades and the air flow interaction and a reasonable computational time length yielded in adoption of a 2D and quasi 2.5D modelling approaches. Those simplifications do not allow for the modelling of the blades edge vortices. Also, to reduce the number of the computational cells no central shaft, support struts and elements were generated. At the investigated range of TSR $\lambda = 0.1 \div 4.5$, the Max Number in the rotor area does not exceed $Ma = 0.3$. Therefore, the fluid flow is assumed to be incompressible. According to the simplifications regarding the investigated turbine, the flow passing through its rotor is assumed to be unsteady and isothermal and the blade walls are assumed to be ideal walls.

3.2. Theoretical Model, Mathematical Apparatus

The incompressible flow passing through the turbine is calculated through the impulse conservation equation and the mass conservation equation. The whole computational area is divided into separate elements (volumes) called cells, which are forming the computational mesh. The governing equations system is calculated for each cell node. The cell nodes are called computational nodes. The computational procedure is iterative and runs until reaching a pre-set accuracy margin.

❖ *Reynolds Averaged Navier-Stokes equations (RANS)*

The RANS flow modelling approach is described as an approximation of a real flow at which none of the vortex structures is directly calculated through the governing equations. The vortex structures generation, detachment and interactions are modelled through the aid of turbulent models. The turbulent structures are introduced into the main flow as time-averaged turbulent fluctuations through the time-averaged Reynolds Navier-Stokes equations. The instantaneous fluctuation component of the velocity can be divided into two types: main (averaged) flow and fluctuating flow (turbulent pulsations).

The velocity fluctuations are generating an additional impulse transfer which is added to the impulse generated by the main velocity components. The time-averaged Reynolds Navier-Stokes equations and the continuity equation for one-dimensional flow are as follow:

(7)
$$\frac{\partial u_i}{\partial x_i} = 0,$$

(8)
$$\frac{\partial}{\partial t}(\rho u_i) + \frac{\partial}{\partial x_j}(\rho u_i u_j - T_{ij}) = -\frac{\partial p}{\partial x_i} + \rho g_i + F_i,$$

where

(9)
$$T_{ij} = \left[\mu \left(\frac{\partial u_i}{\partial x_j} + \frac{\partial u_j}{\partial x_i} \right) \right] - \frac{2}{3} \mu \frac{\partial u_k}{\partial x_k} \delta_{ij} - \overline{\rho u_i' u_j'}.$$

The time-averaged Navier-Stokes equation (8) is further complicated by the addition of a new turbulent term $T_{ij} = -\overline{\rho u_i' u_j'}$, depicting the two additional components of the tangential stress. These additional components are result of the introduction of the fluctuation velocity components. The additional stresses are known as Reynolds Stresses Tensors. The full stress is a sum of the molecular tangential viscous stress and the additional Reynolds stresses.

(10)
$$T_{ij} = -\overline{\rho u_i' u_j'} + \mu \left(\frac{\partial u_i}{\partial x_j} + \frac{\partial u_j}{\partial x_i} \right).$$

The new nine component stress tensor is affected by the fluid properties, the flow parameters such as geometry, velocity, wall roughness and the flow parameters in the area located far away from the zone of interest (undisturbed flow).

❖ **Turbulent Models with Two Equations**

The turbulent models with two equations are incorporating two additional transport equations which allow for the flow turbulence parameters modelling through convection and diffusion of the turbulent kinetic energy. In most of the cases, one of the transport variables is the turbulent kinetic energy k. The other transport variable varies in accordance with the type of the used turbulent model. In most cases, those variables are the turbulent kinetic energy dissipation ε or the specific dissipation ω. The turbulent kinetic energy k depicts the energy of the turbulent structures, while the turbulence kinetic energy dissipation ε and the specific dissipation ω depicts the overall size of the vortex structures.

❖ **Turbulent Model $k - \omega$ SST**

The turbulent model $k - \omega\,SST$ Share Stress Transition (transition of tangential stresses) is a hybrid model. This model combines the advantages of the $k - \varepsilon$ and the $k - \omega$ models. The $k - \varepsilon$ model is applied to the main flow calculation, while for the near wall regions the $k - \omega$ model is used. The $k - \omega\,SST$ model transport equations are presented below.

The specific dissipation is defined as:

(11)
$$\omega = \varepsilon / k$$

where $k = 1/2 \left(\overline{u}' + \overline{v}' + \overline{w}' \right)^2$ is the turbulent kinetic energy, $\varepsilon = k^{3/2} / l$ is the frequency of the kinetic energy dissipation, l is the vortex mixing length.

The turbulent kinetic energy k balance equation is:

(12)
$$\frac{\partial (\rho k)}{\partial t} + \frac{\partial (\rho u_j k)}{\partial x_j} = P - \beta^* \rho \omega k + \frac{\partial}{\partial x_j} \left[(\mu + \sigma_k \mu_t) \frac{\partial k}{\partial x_j} \right].$$

where β^*, σ_k are constants, ω is specific dissipation, μ is molecular viscosity, $\mu_t = \rho C_\mu k^2 / \varepsilon$ is turbulent viscosity.

The first term of the left side of the above equation is accounting for the rate of change in the turbulent kinetic energy k, the second term is convective one accounting for the transfer of k by convection. The first term on the right side of the equation is a source term, accounting for the degree of kinetic energy k generation, the second one is a dissipative term accounting for the rate of k dissipation, the third is diffusive, accounting for the k transfer through diffusion.

The specific dissipation ω equation is:

$$(13) \qquad \frac{\partial(\rho\omega)}{\partial t} + \frac{\partial(\rho u_j \omega)}{\partial x_j} = \frac{\gamma}{\nu_t} P - \beta\rho\omega^2 + \frac{\partial}{\partial x_j}\left[(\mu + \sigma_\omega \mu_t)\frac{\partial \omega}{\partial x_j}\right] + 2(1 - F_1)\frac{\rho\sigma_\omega}{\omega}\frac{\partial k}{\partial x_j}\frac{\partial \omega}{\partial x_j}.$$

Here the first term of the left side of the equation accounts for the rate of change in ω, the second term is convective, accounting for the ω transfer through convection. The first term on the right side of the equation is source term, accounting for the rate of ω generation, the second one is a dissipative term, accounting for the degree of ω dissipation, the third term is diffusive, accounting for ω transport through diffusion and the last one is a mixed-diffusion term which is an additional source term, accounting for the modelling of the transition from ε to ω.

❖ Large Eddy Simulation (LES)

The LES is an advanced CFD simulation approach which overcomes the shortcomings of the RANS modelling. From a mathematical point of view, the LES approach divides the velocity field into two categories – for direct calculation and for sub-grid modelling. The directly solved portion of the flow field includes the large vortex structures, while the modelled sub-grid portion depicts the small vortex structures. The small vortex structures influence over the simulation performance is carried through sub-grid models.

Regarding the instantaneous components of the flow velocity, $\overline{u}$ is the directly calculated term, connected to the large vortex structures, while the $u^{'}$ is the modelled term connected to the small structures. By incorporating the mathematical operation convolution over $u(\vec{x})$ through a filtering function G the modelled fraction of the flow can be determined.

$$(14) \qquad \vec{u}(\vec{x}) = \int_0^\Delta G\left(\vec{x} - \vec{\xi}\right)u\left(\vec{\xi}\right)d\vec{\xi},$$

In the majority of the commercial CFD software produces the LES filtering is spatial dependent and is incorporated through the geometrical parameters of the computational mesh. This means that the computational cell size Δ will have determining role in the LES simulation regarding the overall size of the directly calculated vortex structures.
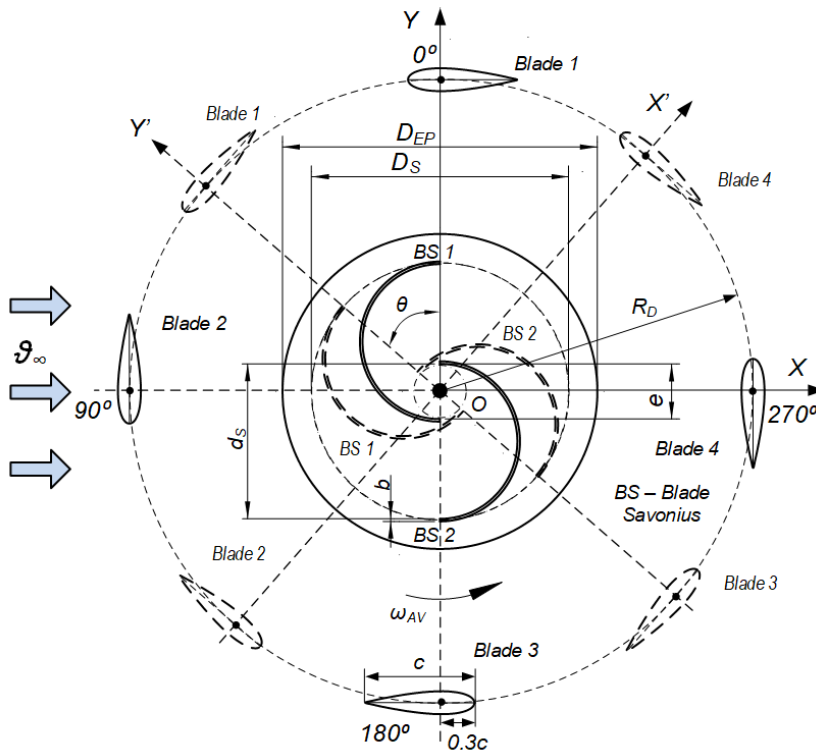
The application of the LES approach over the calculation of the incompressible form of the Navier-Stokes equations imposes that the impulse equation (8) undergoes a change. A filtering regarding the velocity and the pressure is applied. The obtained new equation is:

$$(15) \qquad \frac{\partial \vec{u_i}}{\partial t} + \vec{u_i}\frac{\partial \vec{u_i}}{\partial x_j} = -\frac{1}{\rho}\frac{\partial \vec{p}}{\partial x_i} + \frac{\partial}{\partial x_j}\left(\upsilon\frac{\partial \vec{u_i}}{\partial x_j}\right) + \frac{1}{\rho}\frac{\partial \vec{\tau_{ij}}}{\partial x_j}.$$
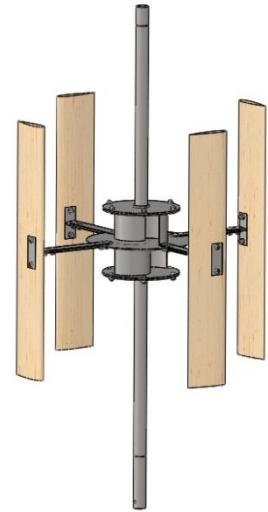
3.3. Theoretical Investigations Methodology

❖ *Properties of the Investigated Wind Turbine*

The investigated configuration of the hybrid turbine is comprised of two wind rotors, Darrieus and Savonius, mounted on a mutual shaft (fig. 5 b). The Darrieus rotor construction variations incorporate tow and four straight blades with a symmetric airfoil section NACA 0021. The blades are mounted on diameter $D_D = 0.4\ m$, around a vertical shaft with blade pitch angle of $\varphi = 0^o$. The Savonius rotor has a double stage construction with diameter of $D_S = 0.1\ m$. The stages are displaced to each other on phase angle of 90°. Each rotor stage is comprised of two semi-circular blades with diameter $d_S = 0.06\ m$. The blades are eccentrically mounted between endplates with diameter $D_{EP} = 0.12\ m$. The ratio between the two rotors radiuses R_S / R_D has a significant influence on the performance of the hybrid turbine. Whit the increase of that ratio the vortex trail produced by the Savonius rotor grows, which leads to drop in the hybrid rotor power coefficient C_P. At ratio $R_S / R_D > 0.3$, the hybrid rotor power coefficient plummets. The hybrid rotor start-up wind speed is also influenced by the ratio R_S / R_D. With the increase of the ratio the torque generated by the Savonius rotor rises, resulting in decrease in the value of the start-up wind speed.

a. Hybrid Rotor Darrieus-Savonius Schematics   *b. 3D Model Darrieus-Savonius*

Fig. 5 Hybrid Wind Rotor Darrieus-Savonius

During the development of the combined rotor design, a solid connection between the two wind rotors was chosen to keep the overall construction relatively simple. The ratio between the rotors radiuses was chosen to be $R_S / R_D = 0.25$. At this ratio, the start-up wind speed is expected to be $\vartheta_\infty < 4.8\ m/s$. The geometrical parameters of the investigated wind rotors are presented in table 1. The computational scheme of the four-bladed hybrid wind turbine is shown in fig. 5 a. The turbine has a rotating coordinate system OX'Y'. The

reference blade is the blade connected to axis OY'. The retorting coordinate system is revolving around an absolute coordinate system OXY. The reference axis is the OY axis. The motion of the rotating system is evaluated through the reference OY axis. The air flow is coming at the wind turbine wit velocity ϑ_∞ along the direction of the OX axis of the absolute coordinate system.
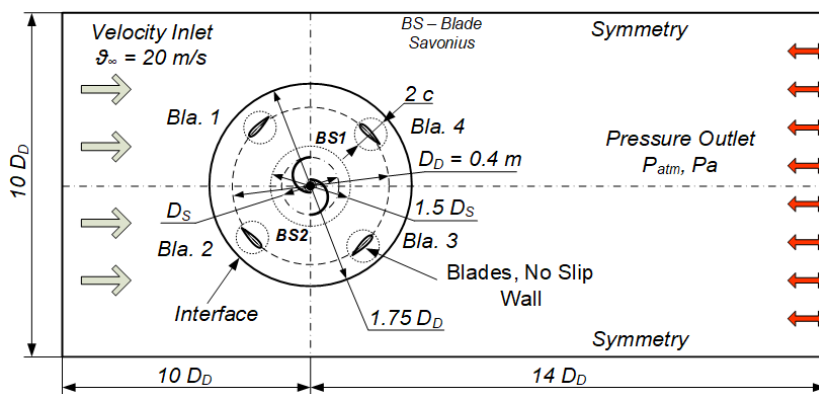
Table 1 Geometrical Parameters of the Rotors

Geometrical Parameters of the Hybrid Wind Rotor					
Darrieus Rotor			*Savonius Rotor*		
Diameter	D_D, m	0.4	Diameter	D_D, m	0.1
Rotor height	H_D, m	0.4	Rotor height	H_D, m	0.1
Number of blades	N, -	2; 4	Eccentricity	e, -	0.35
Chord length	c, m	0.07	Number of blades	N	2; 4
Airfoil section	NACA	0021	Blade thickness	b, m	0.001
Solidity	σ, -	0.35; 0.7	End plate diameters	D_{EP}, m	0.12
Mounting point	MP, m	0.3 c	Blade diameter	d_s, m	0.06
Shaft diameter	d, m	0,02	Shaft diameter	d, m	0.02

❖ *2D Modelling – Computational Domain*

The technique Sliding Mesh was used for the adequate modelling of the turbine rotation. The Sliding-Mesh technique implies the generation of two separate computational zones. The first one is a stationary rectangular zone with a circular opening, which centre aligns with the turbine axis of rotation. This stationary zone depicts the flow field around the wind turbine. The second area is a circular zone, which is enclosing the turbine geometry and rotates with the angular velocity ω_{AV} of the rotor.

The Darrieus, Savonius and Darrieus-Savonius computational domains are presented in fig. 6. The inlet and outlet of the computational domain are placed respectively on 10 diameters in front and 14 diameters behind the wind turbine. This allows for the full development of the air flow. The width of the computational domain is set to be 10 diameters. At the inlet of the computational domain, a velocity inlet boundary condition $\vartheta_\infty = 20\,m/s$ is applied. At the outlet of the computational domain, a pressure outlet boundary condition $p = p_{atm}$ is applied. A Symmetry boundary condition is set over the two horizontal walls of the stationary domain. The blades are treated as ideal walls, so the no-slip wall boundary condition is used. Over the contact area between the two computational zones, an interface boundary condition is applied. This allows for the continuity of the flow through the two separate computational zones.

Fig. 6 Computational Domain and Boundary Conditions

❖ Computational Mesh Parameters

For both 2D computational zones, an unstructured computational mesh is generated. This type of mesh provides sustainable solution accuracy throughout the simulation procedure. The main advantages of the unstructured mesh are its excellent applicability for complex geometry designs, easy setup and manipulation. For all the investigated rotors designs, an unstructured quadrilateral mesh is used for the stationary zone. For the

rotational zone, an unstructured triangular mesh is used. The accuracy of the solution greatly depends on the precise modelling of the flow in the near wall (blades) region, namely the adequate modelling of the boundary laminar sublayer. Therefore, a refined structural quadrilateral mesh was applied for the area of the laminar boundary sublayer. The value of the dimensionless criteria y^+ depicts the quality of the mesh at the near wall regions and the accuracy of the calculations provided by the turbulence model. The y^+ criteria depict the distance from the wall up to the first computational node from the mesh. The near wall criterion is computed as follows:

(16)
$$y^+ = \frac{\rho U_\tau y}{\mu},$$

where ρ is the air density, y is the normal distance from the wall to the first computational node from the mesh, $U_\tau = \sqrt{\tau_\omega / \rho}$ is frictional velocity, $\tau_\omega = \mu(\partial u / \partial y)$ is near wall tangential stress defined through the near wall velocity gradient in normal direction, μ is the air dynamic viscosity. The near wall criteria values in the range of $1 < y^+ < 5$ corresponding to meshes with sufficient densities to allow for the modelling of the laminar boundary sublayer.
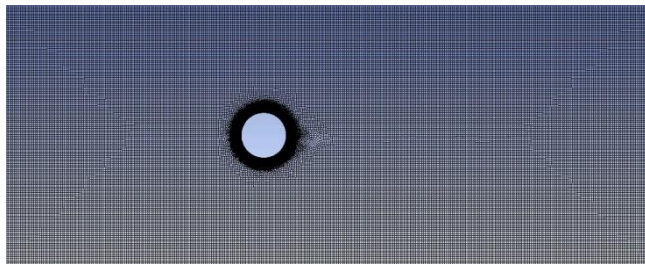
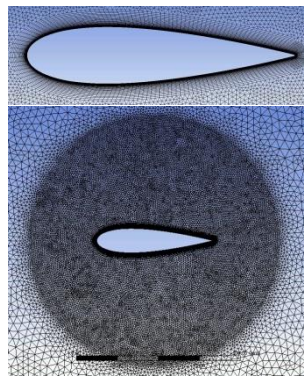| Table 2 Savonius Rotor		Table 3 Darrieus Rotor	
Stationary zone		*Stationary zone*	
Maximum size	10 mm	Maximum size	30 mm
Size at the interface area	2.5 mm	Size at the interface area	5 mm
Rotational zone		*Rotational zone*	
Maximum size	2.5 mm	Maximum size	2.5 mm
Near blade cell size	1 mm	Near blade cell size	1 mm
Cell length on the blade surface	1 mm	Cell length on the blade surface	1 mm
First cells row height	0.01 mm	First cells row height	0.01 mm
Growth rate factor	1.2	Growth rate factor	1.2

The computational cell sizes for the two distinct zones of the computational domain are presented in table 2 for the Savonius rotor and table 3 for the Darrieus rotor. The hybrid rotor computational mesh properties are derived from the properties of the Darrieus and Savonius rotors meshes.

a. Computational Mesh at the Stationary Zone

b. Computational Mesh at the Rotational Area

c. Computational Mesh in the Near Blade Region

Fig. 7 Hybrid Rotor Computational Mesh

The unstructured quadrilateral mesh at the stationary area is presented in fig. 7 a. The mesh density increases towards the contact area between the stationary and the rotational zones. The mesh for the rotational area is shown in fig. 7 b. In this area, an unstructured triangular mesh is used. The unstructured triangular mesh represents more accurately the curved nature of the blades geometry in contrast with the quadrilateral mesh. The mesh density and refinement level increase towards the near blade areas. A structural quadrilateral mesh is used for the laminar boundary layer modelling. The structural mesh allows for the precise control over the first cells row height. The applied first cells row height guaranties values of the near wall criteria lower than $y^+ \leq 5$ (fig. 7 c).

✥ **Numerical Procedure Solver Setup**

The flow through the rotor of the hybrid VAWT is modelled through the incompressible form of the Navier-Stokes equations. The operation of the turbine is characterized by pronounced flow unsteadiness. The low TSR operational regimes have the most predominant unsteady flow nature. Therefore, the unsteady form of the governing equations (7, 8) is used. The additional tangential stresses are introduced through the two-equation (12, 13) turbulence model $k-\omega\ SST$ (Share Stress Transition). A segregate computational scheme is selected for the calculation of the discretized impulse equations combined whit the continuity equation. The coupled pressure-velocity equations are solved through the SIMPLEC (Semi-Implicit Method for Pressure-Linked Equations-Corrected) computational scheme. A second-order upwind scheme is used for the time discretization. For the pressure spatial discretization calculation, the PRESTO! scheme is applied. For all other variables, a second order upwind scheme is adopted. All the applied computational methods and schemes during the solver setup are presented in table 4. All the used options for the solver setup results in computational accuracy of second order in regard to the time and space discretization.

<div align="center">

Table 4 Solver Setup

</div>

Computational Parameters	Computational Scheme
Pressure-Velocity Coupling Scheme	SIMPLEC
Spatial Discretization Gradient	Last Square Cell Based
Spatial Discretization Pressure	PRESTO!
Spatial Discretization Momentum	Second Order Upwind
Spatial Discretization Turbulent Kinematic Energy	Second Order Upwind
Spatial Discretization Turbulent Dissipation Rate	Second Order Upwind
Transient Formulation	Second Order Upwind

The selected value for the time step size corresponds to angular rotation of the wind rotor $\Delta\theta = 1^o$. The numerical results were saved at every 10th time stem to reduce the volume of the computational data. The pre-set number of the inner iteration per timestep is 100. This guaranties Scaled Residuals solution convergence at the order of 10^{-4} (Scaled Residuals≤10^{-4}).
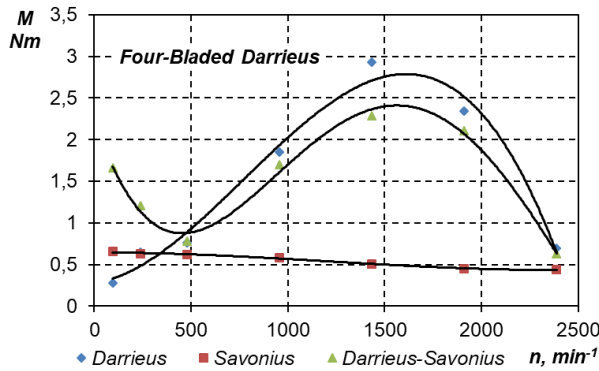
3.4. Theoretical Results Analysis

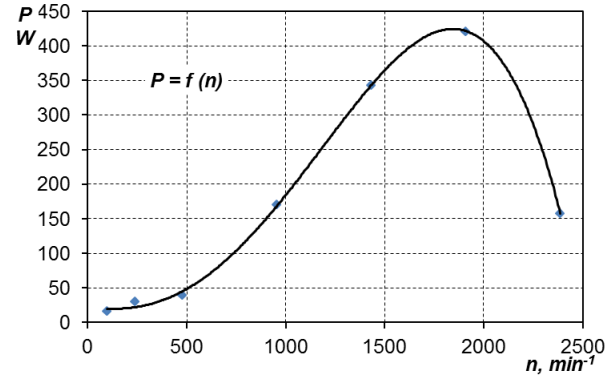✥ **Darrieus-Savonius Hybrid Rotor Numerical Results – Four-Bladed Darrieus**

The torque performance characteristics for each of the hybrid turbine comprising rotors are shown on fig. 8 a. In the range of low RPM $n < 500$ min^{-1} the Darrieus rotor has insignificant start-up torque value, whereas the hybrid rotor configuration reaches values of around $M_{ST} \approx 2\ Nm$. The start-up torque of the hybrid turbine is provided by the Savonius rotor. The Savonius rotor has a rigid torque characteristic, which does not change significantly with the rise of the RPM. With the increase of the RPM above $n > 500$ min^{-1} the Darrieus performance influence is becoming predominant, while the Savonius performance effect over the hybrid rotor performance is diminishing. The hybrid turbine is combining the performance characteristics of its comprising rotors. Due to this combination, the hybrid rotor torque generation at the range of the high RPM $n > 500$ min^{-1} has lower values in comparison with the Darrieus rotor. The Savonius rotor performance influence over the hybrid configuration has a positive side. It acts as an aerodynamic brake protecting the hybrid rotor from reaching critical RPM, which could lead to the turbine destruction.

The hybrid turbine performance characteristics are not obtained through the superposition method of combining its comprising wind rotors characteristics. The interaction of the flow passing through the comprising rotors is favourable and leads to the formation of a hybrid wind rotor, which has its own distinctive performance characteristics. The hybrid turbine torque curve has a col at TSR $n = 500$ min^{-1}. With the rise of the RPM to

$n = 1,600\,\text{min}^{-1}$ the torque curve forms a rising slope, due to the predominant influence of the Darrieus lift force operational principal. The further increase of the RPM leads to the formation of a falling slope torque curve area due to the increase of the rotor solidity. The rise in the solidity results in increased vortex generation, therefore to larger hydraulic losses.
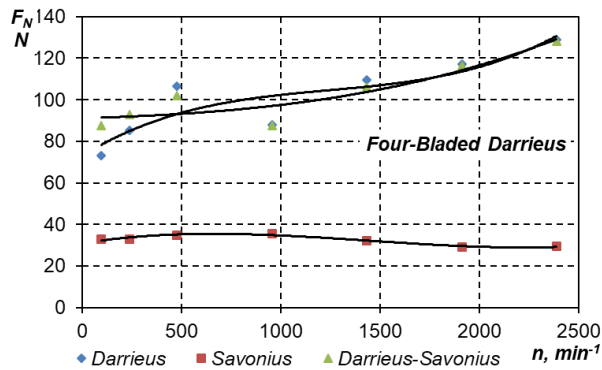

a. Torque Generated by the Hybrid Turbine comprising Rotors

b. Power Output Performance Characteristic

Fig. 8 Hybrid Turbine Performance Characteristics – Four-Bladed Darrieus Rotor

The output power performance characteristic of the hybrid rotor is presented in fig. 8 b. The power curve has a clearly formed maximum and two steep slopes - ascending and descending. The power curve maximum is called nominal power performance point. The nominal power of $P_N \approx 420W$ is reached at nominal RPM of $n_N \approx 1,900\,\text{min}^{-1}$. At the maximum value of the RPM $n_{\max} \approx 2,500\,\text{min}^{-1}$, the hybrid wind rotor generates zero power output. The shape of the power performance curve (narrow operational RPM area) is explained by the rotor high solidity $\sigma = 0.7$. The influence of the Savonius rotor over the hybrid turbine performance as an aerodynamic brake is contributing to the solidity effect.

Fig. 9 Drag Force Generated by the Hybrid Turbine Comprising Rotors
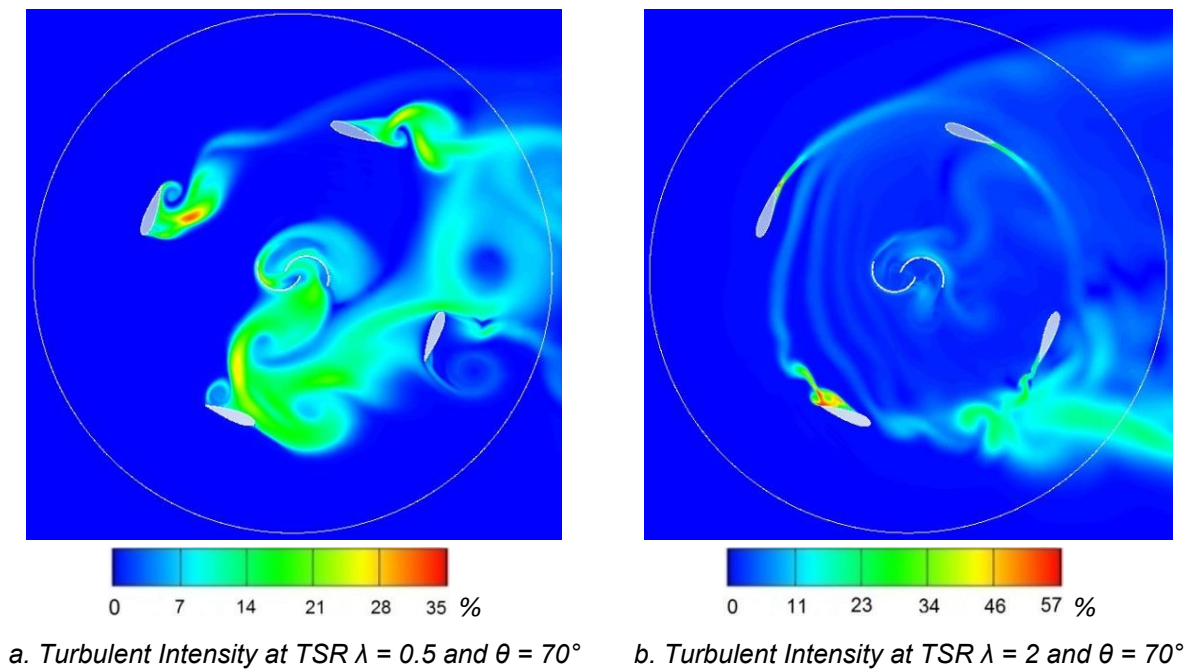
The drag force acting over each of the hybrid turbine comprising rotors is presented on fig. 9. The drag force characteristic curve acting over the Savonius rotor has a relatively linear trend due to which the force is relatively constant. The Savonius drag force is fluctuating in the rage of $F_{NS} = 30 - 35\ N$. At low RPM below $n < 500\ \text{min}^{-1}$ the Darrieus drag force has lower values in comparison with the hybrid rotor drag force. This is due to the Savonius rotor influence over the flow passage through the hybrid turbine as an additional hydrodynamic drag. At higher RPM $n > 500\ \text{min}^{-1}$ the drag curves of both the Darrieus and the hybrid rotors are overlapping. This is due to the decrease in the combined rotor permeability which forces the flow to pass around the turbine. As a result, the flow velocity passing through the rotor decreases. The Savonius drag force effect over the combined rotor diminishes. The Darrieus drag force component is fluctuating in the range of $F_{ND} = 70 - 130\,N$.

The hybrid rotor drag force performance curve has a relatively linear ascending trend. The drag force fluctuates in the range of $F_{NX} = 90 - 130\,N$. The drag performance characteristic has two distinct operational points. The first one is the zero RPM point at which

the drag has value $F_{N_0} = 90\,N$. The latter is the nominal performance point at which the drag force has a value of $F_{N_N} = 105\,N$ reached at $n_N = 1{,}500\,\text{min}^{-1}$. The increase in the drag force generation with the rise of the RPM is explained by the decrease in the combined rotor permeability.

Flow visualization of the flow passing through the hybrid rotor at TSR $\lambda = 0.5$ and $\lambda = 2$ is shown in fig. 10. The turbulent intensity fields for rotor angular position of $\theta = 70^\circ$ being visualized. The main differences between the two operational regimes can be found in the vortex generation intensity and the Darrieus rotor permeability. At TSR $\lambda = 0.5$ (fig. 10 a) massive vortex structures are being generated and shed from both comprising rotors. The vortex generation peaks during the Darrieus rotor blades passage through the downstream area. The detached vortices are mixing and interacting with each other. The combined vortex structures are increasing the hydraulic losses and reducing the power transfer from the air flow to the turbine blades. At operational regime TSR $\lambda = 2$ (fig. 10 b) the flow stays attached to the Darrieus rotor blades and the vortex generation rate is low. At this regime the hybrid rotor solidity increases, the permeability decreases due to the high angular velocity. As a result, the airflow is passing around the hybrid turbine. This is cutting off the Savonius rotor from the main flow, resulting in reduction of the vortex structures produced by it and respectively decrees in the hydraulic losses.
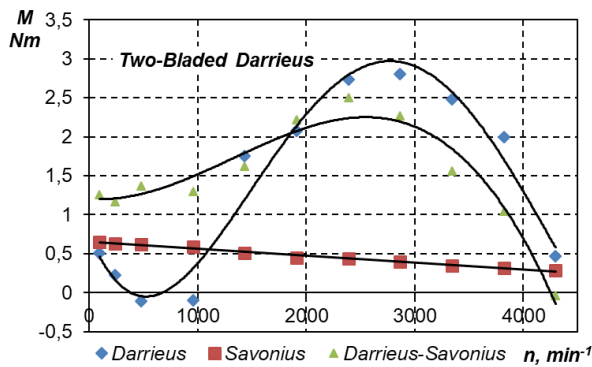

a. Turbulent Intensity at TSR λ = 0.5 and θ = 70°   *b. Turbulent Intensity at TSR λ = 2 and θ = 70°*

Fig. 10 Flow Visualization Through the Darrieus-Savonius Hybrid Rotor – Four-Bladed Darrieus

❖ *Darrieus-Savonius Hybrid Rotor Numerical Results – Four-Bladed Darrieus*
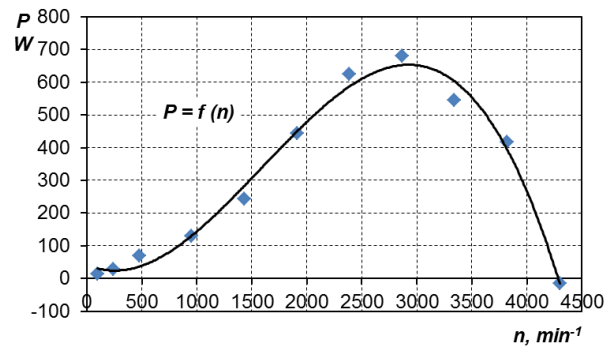
The torque operational characteristics for each of the hybrid turbine comprising rotors are presented in fig. 11 a. At the operational area of low RPM $n < 1{,}500\,\text{min}^{-1}$, the Darrieus rotor has low start-up torque $M_{D_{ST}} = 0.5\,Nm$. The same rotor even reaches negative torque values in the TSR operational area of $500\,\text{min}^{-1} < n < 1{,}000\,\text{min}^{-1}$. As a contrast to the Darrieus torque, the hybrid rotor torque is three times bigger at the same RPM range $M_{H_0} = 1.5\,Nm$. The Savonius rotor is the main contributor to the hybrid rotor start-up capabilities, due to its excellent start-up torque $M_{S0} = 0.7\,Nm$. The Savonius torque has a

rigid trend, fluctuating within a narrow margin $M_S = 0.7 - 0.3\ Nm$ throughout the whole operational diapason of RPM $n = 0 - 4{,}500\ min^{-1}$. The Darrieus rotor operation starts to be predominant at the range of RPM $n = 1{,}100 - 4{,}200\ min^{-1}$. At this operational range, the larger fraction of the hybrid turbine torque is generated by the Darrieus wind rotor. At these regimes, the Savonius rotor is operating as an aerodynamic brake. Due to which the torque generated by the hybrid turbine torque is lower in comparison with the Darrieus rotor at the same operational zone. The positive side of the Savonius rotor acting as a break is the RPM self-regulating ability. It protects the combined wind turbine from reaching dangerously high RPM at high wind speeds.

It is important to be noted that the hybrid turbine operational characteristic is not obtained through the superposition principle applied for its comprising wind rotors. Therefore, the interaction of the flow passing through the comprising rotors is favourable and yields into the creation of a new wind rotor with distinct new properties. As can be seen from the chart the two-bladed Darrieus configuration of the hybrid turbine reaches higher values of the RPM $n_{max} = 4{,}300\ min^{-1}$ in comparison with the four-bladed configuration $n_{max} = 2{,}300\ min^{-1}$. This is due to the two-bladed configuration lower solidity $\sigma_{2Bl} = 0.35$ in comparison with the four-bladed configuration solidity $\sigma_{4Bl} = 0.7$.
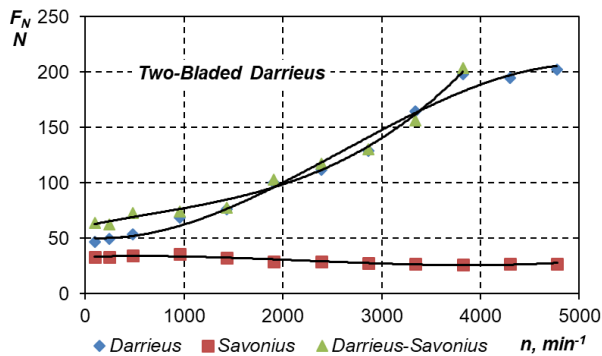

a. Torque generated by the hybrid turbine comprising rotors

b. Power output performance characteristic

Fig. 11 Hybrid Turbine Performance Characteristics – Two-Bladed Darrieus Rotor
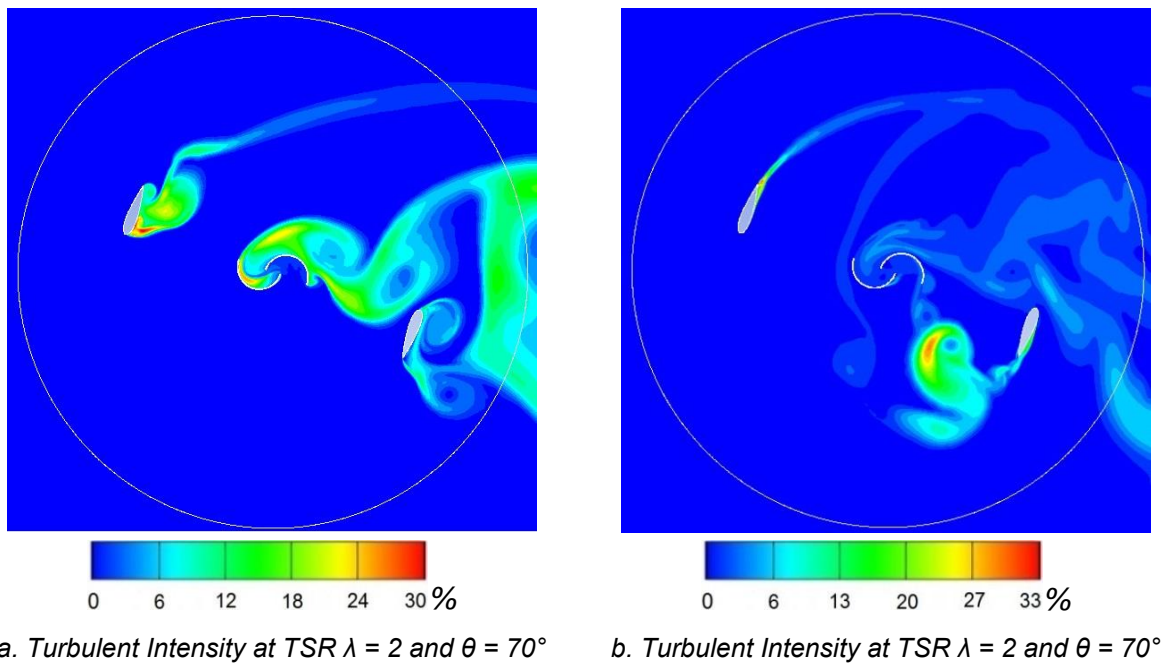

Fig. 12 Drag Force Generated by the Hybrid Turbine Comprising Rotors

The output power performance characteristic of the hybrid turbine is presented in fig. 11 b. The maximum of the characteristic is called a nominal operation point. The nominal output value of the hybrid rotor is $P_N \approx 670\ W$ reached at RPM $n_N \approx 2{,}850\ min^{-1}$. The other distinct operational point corresponds to the turbine maximum RPM $n_{max} \approx 4{,}300\ min^{-1}$ at which zero output power is generated. According to fig. 11 a, the nominal torque $M_N \approx 2.2\ Nm$ corresponds to the nominal value of the RPM. The hybrid rotor low solidity $\sigma = 0.35$ is the main factor that drives the shape of the power curve – a smooth ascending and descending branches with wide range of operational RPM locked between them. The Savonius rotor influence over the passing through flow attributes to the hybrid turbine solidity effect.

The drag force performance characteristic for each of the hybrid turbine comprising rotors is shown in fig. 12. As can be seen from the chart at low RPM $n < 1,000$ min^{-1} the Darrieus drag force has lower values in comparison with the hybrid turbine drag force. The higher values of the hybrid turbine drag force are due to the influence of the Savonius rotor over the passing flow as an additional aerodynamic drag. With the rise of the RPM $n = 1,000 - 3,000$ min^{-1}, an overlapping in both Darrieus and the hybrid rotors characteristics is observed. At RPM $n > 3,000$ min^{-1} the permeability of the two comprising rotors decreases which forces the airflow to pass around them. The decrease in the Darrieus rotor permeability results in the drop of the mass flow rate and flow velocity passing through the hybrid turbine. The solidity decrease is reducing the value of the pressure difference between the total pressures acting on both sides of the Savonius rotor. Due to which the drag force acting over it is diminishing. In this case, it can be concluded that the hybrid turbine performance characteristic is not obtained through the superposition method applied for the comprising rotors.

a. Turbulent Intensity at TSR λ = 2 and θ = 70°   *b. Turbulent Intensity at TSR λ = 2 and θ = 70°*

Fig. 13 Flow Visualization Through the Darrieus-Savonius Hybrid Rotor – Two-Bladed Darrieus
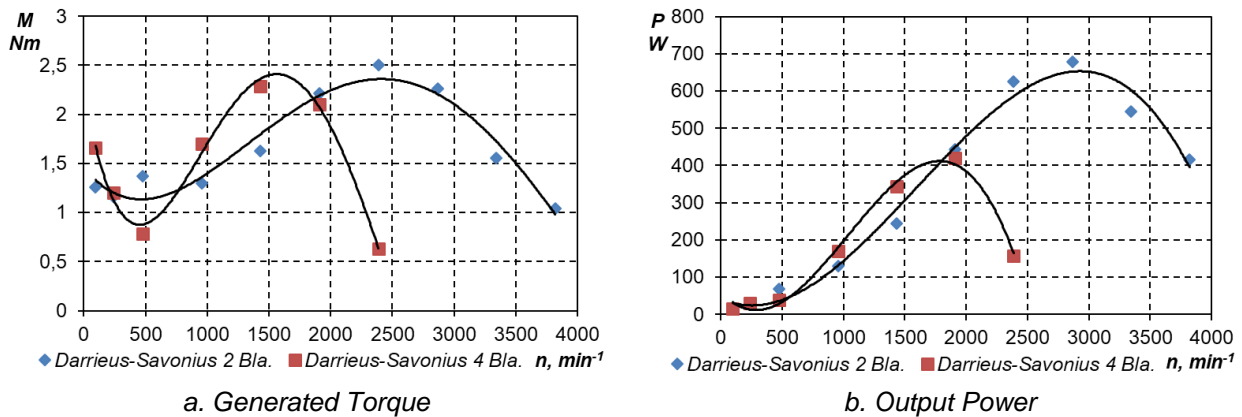
The flow visualization at two different operational regimes $\lambda = 0.5$ and $\lambda = 2$ is shown in fig. 13. The turbulence intensity fields are visualized at the hybrid rotor angular position of $\theta = 70°$. The main differences between the two operational regimes can be found in the intensity of the vortex generation during the blades passage through the upstream and downstream turbine areas. Also, the influence of the Savonius rotor over the main flow passing through the hybrid turbine is noticeable. At TSR $\lambda = 0.5$ (fig. 13 a) a massive vortex structure is formed during the Darrieus blade passage through the upstream area. This structure subsequently detaches from the blade, travels downstream and interacts with the vortices generated by the Savonius rotor. The combined vortex structures are travelling through the downstream area and interfering with the Darrieus blades passing through it. This lowers the energy extraction in the downstream area of the rotor. At TSR $\lambda = 2$ and rotor, the angular position of $\theta = 70°$ (fig. 13 b) the flow is attached to the Darrieus rotor blades. The intensity of the vortex generation is low. The vortex sizes generated by the Savonius rotor are considerably smaller, with lower intensity. Besides that, they are still contributing to the vortex generation and interaction in the downstream turbine area. Due to

which the hydraulic losses in that area are rising. At both operational regimes, there is vortex structures generation and interaction through all the hybrid turbine swept area. Due to which the hydraulic losses are rising, most noticeably at the low TSR operational regimes.

❖ *Comparison Between the Two-and Four-Bladed Darrieus Hybrid Turbine Configurations Theoretical Results*

A comparison between the torque performance characteristics of the two-bladed and the four-bladed configurations of the hybrid turbine is presented in fig. 14 a. As can be seen from the chart both hybrid turbine configurations have excellent self-starting capabilities. The torque generated by both rotors at the area of the low RPM $n < 500$ min^{-1} is in the range of $M = 1 - 1.5$ *Nm*. The four-bladed configuration torque curve forms a col with a minimum reached at $n = 500$ min^{-1}. At the RPM range of $n = 250 - 750$ min^{-1} the influence of the Savonius rotor drag, operational principal over the hybrid turbine torque generation diminishes, whereas the Darrieus lift operational principle surges.
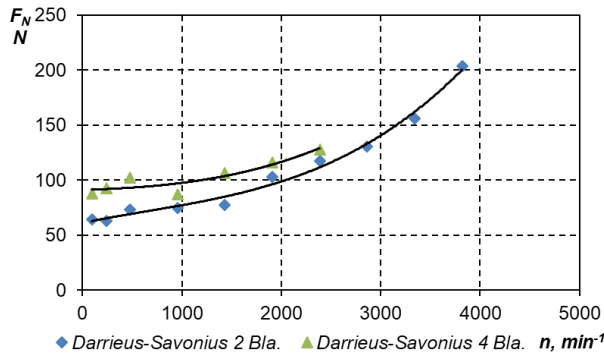
With the increase of the hybrid turbine RPM, the Darrieus rotor blades are beginning to rotate with a peripheral velocity higher than the airflow velocity. This reduces the turbine permeability, therefore the mass flow rate through the hybrid rotor drops. This results in a decrease of the Savonius rotor torque generation. Ultimately this leads to decrease of the hybrid wind turbine total torque. Due to its lift force, operational principal the Darrieus rotor begins to dominate in the process of energy extraction at RPM $n > 500$ min^{-1}. This leads to increase of the total hybrid turbine torque. In the case of the four-bladed configuration the torque increase until reaching its maximum of $M_{max} = 2.3$ *Nm* at $n = 1{,}700$ min^{-1}. In the case of the two-bladed configuration, the torque rises until reaching its maximum of $M_{max} = 2.5$ *Nm* at $n = 2{,}500$ min^{-1}. The two-bladed hybrid rotor configuration characteristic has a distinct shape at the area of low RPM $n < 750$ min^{-1} in comparison with the four-bladed configuration. The torque generated in this area of RPM stays relatively constant with a value of around $M \approx 1.3$ *Nm*. At the two-bladed turbine configuration, the transition from the Savonius dominant operational range of RPM to the dominant range of the Darrieus rotor is smooth. The main portion of the hybrid turbine torque is generated by the Darrieus rotor at RPM $n > 1{,}000$ min^{-1}. The low solidity of the two-bladed Darrieus rotor is the main factor which contributes to the favourable compilation of the hybrid turbine comprising rotors. The overall shape and behaviour of the characteristics are predetermined by the rotors solidity. The peculiarity in both hybrid configurations is the contribution of the Savonius rotor to the rise of the solidity effect over their performances.

a. Generated Torque

b. Output Power

Fig. 14 Torque and Output Power Performance Characteristics

A comparison between the power performance characteristics of both the two-bladed and the four-bladed hybrid turbine configuration is shown in fig. 14 b. The four-bladed rotor configuration generates power effectively in a narrow operational area of RPM $n = 1,000 - 2,300$ min^{-1}. The maximum value of the power output for this configuration is $P_{max} \approx 420$ W reached at nominal RPM of $n_N \approx 1,900$ min^{-1}. The two-bladed rotor configuration generates effectively output power in a wider range of RPM $n = 1,000 - 3,800$ min^{-1} in contrast to the four-bladed one. The maximum power output reached this configuration is $P_{max} \approx 680$ W at nominal RPM of $n_N \approx 2,800$ min^{-1}. The four-bladed hybrid configuration generates larger amounts of power in the operational area of RPM $n < 2,000$ min^{-1} in comparison with the two-bladed configuration.

A comparison between the drag force performance characteristics for both variations of the two-bladed and the four-bladed hybrid turbine is shown in fig. 15. At the operational area of RPM $n < 2,000$ min^{-1}, the drag force acting on the four-bladed configuration of the hybrid turbine is greater in comparison with the two-bladed one. The difference in the drag force between the two variations of the hybrid rotor is due to the difference in the rotors solidity. In both hybrid turbines configurations, the Savonius rotor is contributing to the domination of the solidity effect over their performance. The high solidity of the four-bladed hybrid configuration obstructs the flow passage through the wind rotor and forces it to pass around the turbine. This yields into the formation of two separate areas in front and behind the rotor with large total pressure difference between them.

Fig. 15 Hybrid Turbine Drag Force

This results in increase of the drag force acting over the four-bladed hybrid turbine. The rise of the rotational velocity of the rotor is favouring the rise of the solidity effect. The drag curves for both hybrid turbine configurations have similar trends. The drag force is increasing with the rise of the angular velocity. The difference in the drag force values is diminishing after passing RPM of around $n \approx 2,000$ min^{-1}. Based on the drag force characteristics, it can be concluded that influence of the solidity over the drag force values is diminishing after reaching RPM higher than $n > 2,300$ min^{-1}.

3.5 Theoretical Analysis Conclusions

Based on the conducted theoretical results analysis the following conclusions are made:

1. The proposed CFD methodology is an adequate tool for vertical axis wind turbines performance prediction and operation analysis. The 2D CFD modelling approach successfully simulates the formation, development and interaction of the complex vortex structures detaching from the turbine blades surfaces.

2. The 2D URANS numerical approach results in the modelling of large homogenous vortex structures due to its operational principle – time averaging of the turbulent pulsations. On the other hand, the 2.5D LES numerical approach provides more realistic modelling of the vortex structures generation and dissipation rates. In this approach, the large vortex structures are calculated directly through the governing equations, while the small structures are modelled. The 2.5D LES numerical approach has high demands towards the computational hardware and the computational mesh density. The result of those demands is an extremely long computational time which is limiting the 2.5D LES approach application.

3. A numerical independence study over some computational parameters was conducted. It is established that the periodicity of the theoretical result is reached after the fifth full revolution of the investigated turbine. Furthermore, it is established that the values of the near wall criteria y^+, ensuring the modelling of the boundary laminar sublayer are lower than $y^+ < 5$ for all the modelled turbines.

4. The Darrieus rotor with solidity of $\sigma = 0.7$ (four blades) has a maximum power coefficient of $C_{P_{max}} \approx 0.25$ reached at TSR $\lambda \approx 2$. The maximum drag coefficient of the four-bladed rotor is $C_{FN_{max}} \approx 1.3$ reached at TSR $\lambda = 2.5$. The Darrieus rotor with solidity $\sigma = 0.35$ (two blades) has maximum power coefficient of $C_{P_{max}} \approx 0.44$ reached at TSR $\lambda \approx 3.5$. The maximum drag coefficient of the two-bladed rotor is $C_{FN_{max}} \approx 2.1$ reached at $\lambda = 4.5$.

5. The hybrid turbine comprising rotors are interacting with each other on multiple levels. The result is a new hybrid configuration turbine with superior self-starting capabilities regarding its comprising rotors. With the increase of the hybrid turbine RPM, the Savonius rotor begins to act as an aerodynamic break, preventing the hybrid configuration from reaching dangerously high RPM. As a part of the hybrid configuration, the Savonius rotor favours the rise of the solidity effect over the turbine operation. This results in increase of the drag force coefficient and drops in the power coefficient. The two-bladed Darrieus hybrid rotor configuration has better self-starting capabilities and is more efficient in contrast with the two-bladed Darrieus configuration.

6. The four-bladed Darrieus hybrid turbine configuration has a maximum power coefficient of $C_{P_{max}} \approx 0.21$ reached at $\lambda \approx 2$. The maximum drag coefficient of the four-bladed configuration is $C_{FN_{max}} \approx 1.3$ reached at $\lambda = 2,5$. The two-bladed Darrieus hybrid turbine configuration has a maximum power coefficient of $C_{P_{max}} \approx 0.34$ reached at $\lambda \approx 3$. The maximum drag coefficient of the two-bladed configuration is $C_{FN_{max}} \approx 2.1$ reached at $\lambda = 4$.

4. CHAPTER EXPERIMENTAL INVESTIGATIONS

4.1. Experimental Investigation Methodology and Test Bench Schematics
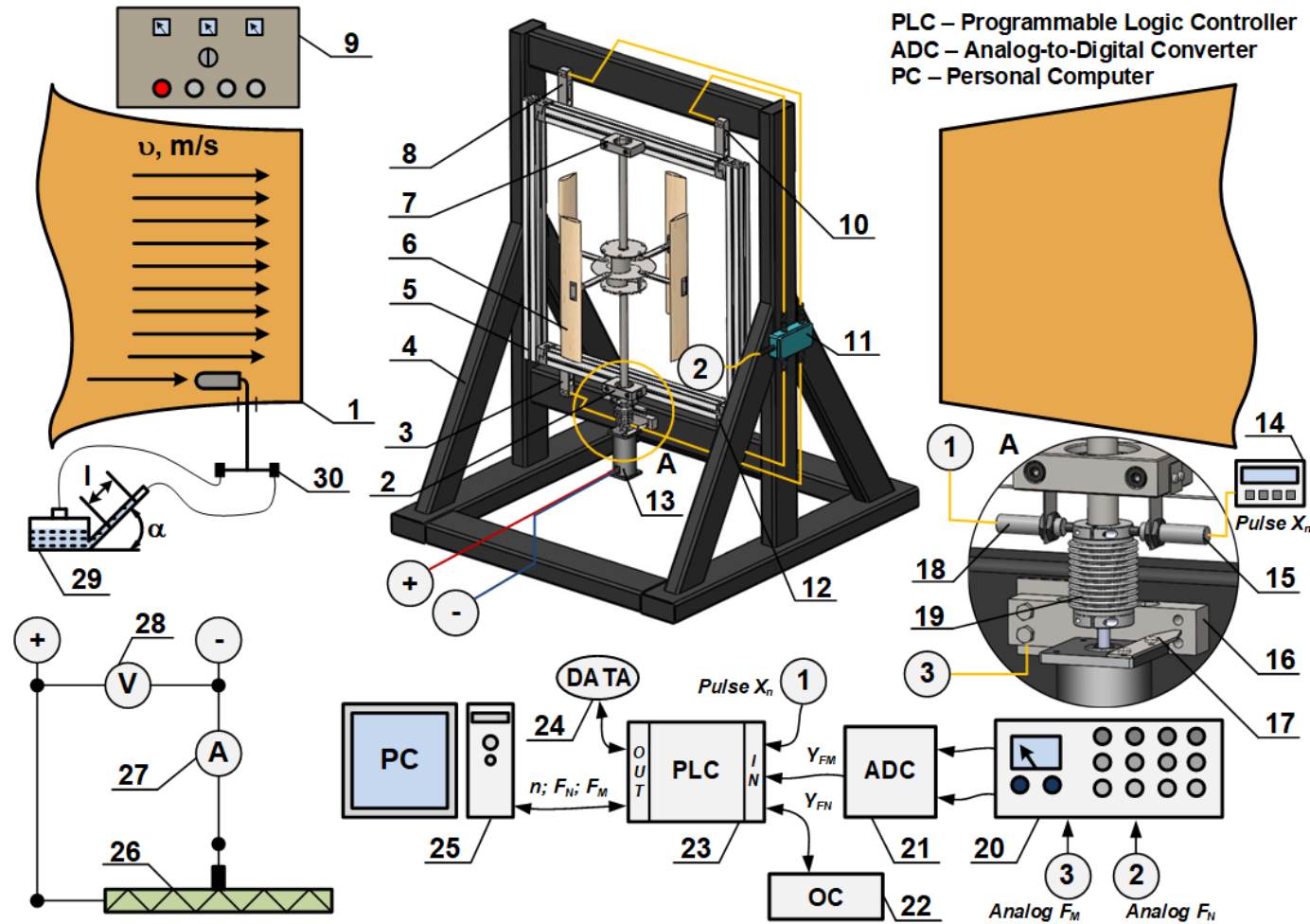
The schematics of the developed VAWT test bench is presented in fig. 16. The test bench is placed inside a closed couture type wind tunnel (1) uncovered operational area. The wind tunnel operational area dimensions are 0.45 x 0.45 x 0.765 m. The air velocity in the wind tunnel operational zone can be regulated in the range of $0 \div 40$ m/s through the change of an axial fan rotational speed. The air flow measurement is accomplished through a measurement scheme Prandtl tube (30) and differential micromanometer (29).

The experimental investigation of the wind turbine (6) performance characteristics begins with the set of the air flow velocity ($\upsilon_i = const$) from the wind tunnel console (9). The measurement of the drag force F_N acting on the wind turbine is accomplished through its mounting in the wind tunnel (1) operational area on an aluminium frame (5) which is attached to a support frame (4) by the aid of four force transducers/load cells (3), (8), (10) and (12). The drag force is transferred through the aluminium frame to the force transducers. The transducers are transforming the input force into analogue electrical signals (Analogue A_N). The signals are relayed to a signal unifying box (11), where their values are averaged and summed up. The unifying box (11) output averaged signal is passed to a signal amplifier (20) which is transforming the input signal into a standard output analogue signal $0 \div 20 \, mA$. Afterwards the standard signal is relayed to an Analogue-to-Digital Converter (21, ADC) which discretizes and transforms the signal into a 12-bit number Y_{FN}. This number is then transferred to a Programmable Logic Controller (23, PLC) which through a predefined transformation $F_N = f(Y_{FN})$ function is transformed into the signal Y_{FN}. The Y_{FN} signal is directly connected to the drag force F_N. The drag force can be visually monitored on the signal amplifier (20) analogue display.

The operational console (22, OC) connected to the PLC is used for the custom data registering software setup and management. It is also used for nullification of the independent PLC memory (24, DATA). The PLC operation is monitored by the PC (25), which is also used for downloading the acquired data from the PLC memory (24).

A DC generator (13) connected to the wind turbine (6) shaft through a precise bellow coupling (19) is used for the torque production M measurement. The wind turbine torque drives the production a reactive torque in the DC generator (13) stator. Through a rod (17) attached to the DC generator stator, the reactive torque is converted to a pressure force acting on a load cell (16). The load cell is converting the pressure force into an analogue electrical signal (Analog A_{FM}). Afterwards, the signal is transmitted to the signal amplifier (20) where it is converted to a standard analogue signal $0 \div 20 \, mA$ and it is passed to the Analogue-to-Digital Converter (21, ADC). The ADC (21) discretizes the signal into a 12-bit number Y_{FM}.

The standard ADC output signal is passed to the PLC (23) where through a pre-set transformation function $F_M = f(Y_{FM})$ it is converted to the force F_M. The Y_{FM} signal is directly connected to the force F_M generated by the reactive torque. The wind turbine torque can be visually monitored on the signal amplifier (20) analogue display.

Fig. 16 Schematic of the Developed VAWT Investigation Test Bench

1 – Wind Tunnel with an open operational area; 2, 7 – Bearing Housings; 3, 8, 10, 12, 16 – Load Cells; 4 – Support Frame; 5 – Aluminium Frame; 6 – Hybrid Rotor Darrieus-Savonius; 9 – Wind Tunnel Operation Console; 11 – Signal Unifying Box; 13 – DC Generator; 14 – Frequency Meter; 15, 18 – Inductive Proximity Sensors; 17 – Rod; 19 – Precise Bellow Coupling; 20 – Signal Amplifier; 21 – Analogue-to-Digital Converter – ADC; 22 – Operational Console; 23 – PLC; 24 – Independent PLC Memory; 25 – PC; 26 – Load Device(Rheostat); 27 – Amperemeter; 28 – Voltmeter; 29 – Differential Micromanometer; 30 – Prandtl Tube.

A couple of metal pins are mounted on the bellow coupling (19) periphery. They are acting as trigger devices for the two Inductive Proximity Sensors (15) and (18). The two Inductive Proximity Sensors are converting the rotational speed (RPM) of the wind turbine shaft into impulse electrical signal (Pulse X_n). The signal from one of the sensors is transmitted to a frequency meter (14) for a visual reading. The signal from the other sensor is transmitted to the PLC (23).

A rheostat (26) is used as a load device for the DC generator, respectively for the wind rotor. For each established operational regime ($v_i = const, n = const$) of the wind turbine, the rotor parameters (F_N, Mn) are being automatically written in the PLC independent memory. The load is being gradually increased until overload of the wind rotor is reached i.e. until the rotor reaches zero RPM. The values of the electric current and the tension in the DC generator load circuit are monitored by a voltmeter (28) and an amperemeter (27).

4.2. Investigated Wind Rotors Geometrical Parameters

The schematics of the experimental hybrid wind turbine Darrieus-Savonius is presented in fig. 17. The hybrid rotor construction allows for a robust change of the blades number and their pitch angle. The configuration can easily be modified from a hybrid to a Savonius rotor after disassembly of the Darrieus rotor blades. The main geometrical parameters of the experimental hybrid configuration are presented in table 5.
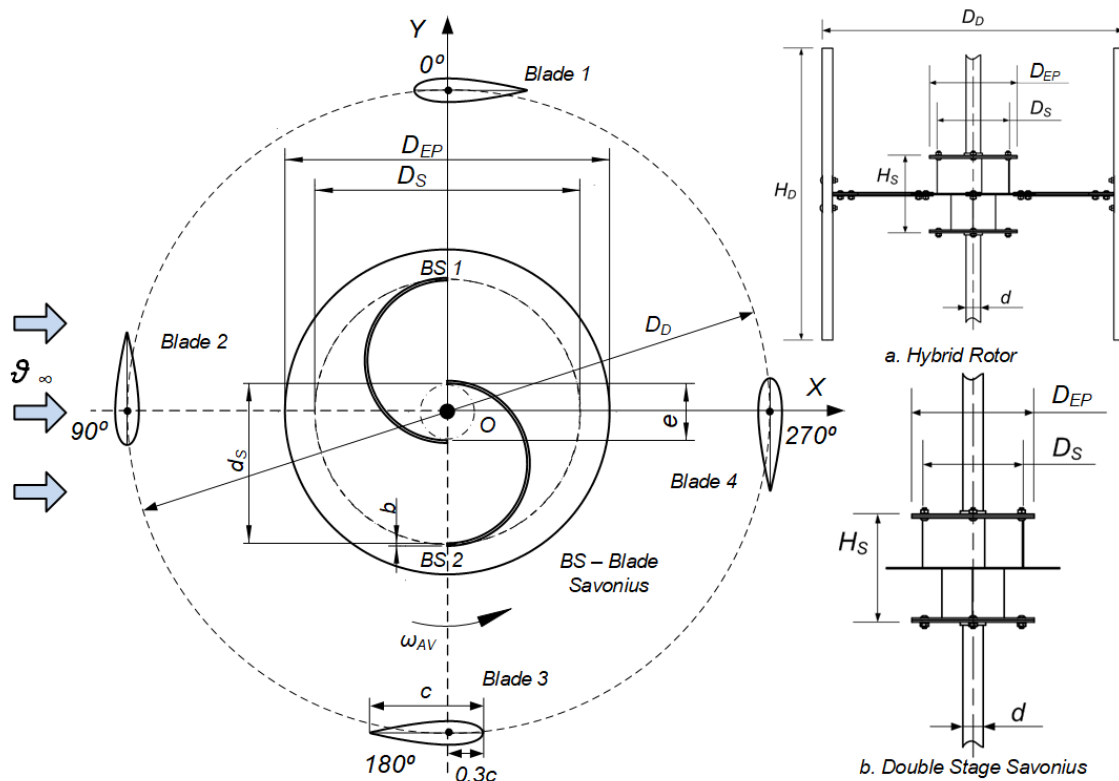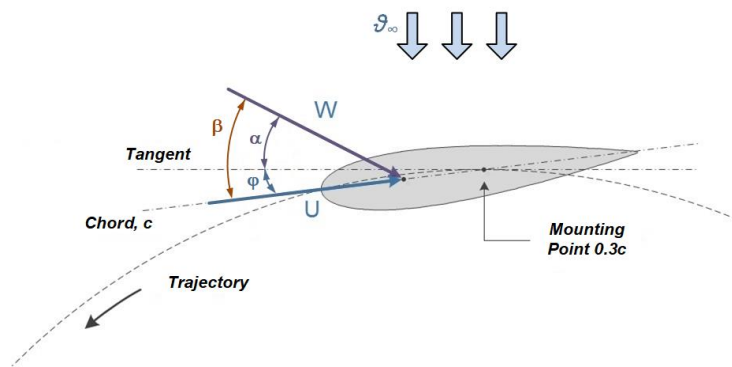

Fig. 17 Schematics of the Experimental Hybrid Wind Turbine Darrieus-Savonius

The blade pitch angle φ is formed between the blade chord and the line tangential to the circular blade trajectory (fig. 18). When the front half of the blade is tilted towards the rotor centre of rotation the pitch angle has a positive value. This position is also called toe in tilt. When the front half of the blade is tilted outward the rotor centre of rotation (toe out tilt) the pitch angle has negative value. The schematics are shown in fig. 18 depicts the

relation between the pitch angle φ and the angle of attack α- $\beta = \alpha + (\pm\varphi)$. The positive values of the pitch angle lead to an increase in the angle of attack values $\alpha = \beta + \varphi$, whereas the negative pitch values result in a decrease of the angle of attack values $\alpha = \beta - \varphi$. When the pitch angle value is $\varphi = 0°$, then the angle of attack value is $\alpha = \beta°$. The relation between these angles determines the flow kinematics through the wind rotor and the aerodynamic forces ratios.

Table 5

Geometrical Parameters of the Hybrid Rotor						
Darrieus Rotor			**Savonius Rotor – Double Stage**			
Diameter	D_D, m	0,4	Diameter	D_S, m	0,1	
Rotor Height	H_D, m	0,4	Rotor Height	H_S, m	0,1	
Blade Number	N, -	2; 3; 4	Eccentricity	e, -	0,35	
Chord Length	c, m	0,07	Blade Number Per Stage	N, -	2	
Airfoil Section	NACA	0021	Blade Thickness	b, m	0,001	
Solidity	σ, -	0,35; 0,525; 0,7	End Plates Diameter	D_{EP}, m	0,12	
Mounting Point	MP, m	0,3c	Blades Diameter	d_S, m	0,06	
Shaft Diameter	d, m	0,02	Shaft Diameter	d, m	0,02	

Fig. 18 Blade Pitch Angle

The Savonius rotor acts as a mounting hub in the hybrid configuration. The Darrieus blades are mounted to the hub (Savonius rotor) through struts and joints (fig. 17). The Darrieus rotor blades pitch angle φ is changed through their rotation at the strut-to-blade mounting joint. The physical rotation of blades in the current experimental turbine is achieved through the change of the supporting struts. Each set of struts have specifically displaced to each other mounting openings. After mounting the blades with a given set of struts a different pre-set pitch angles are achieved. The investigated pitch angles are $\varphi = -16° \; -6°, \; 0° \; 6° \; \text{and} 16°$.

The investigated turbine solidity is altered through the change of the Darrieus rotor blades number $N = 2, 3, 4$. The airfoils chord length is kept constant for all variations of the investigated hybrid rotor design. According to equation (5) the corresponding turbine solidities are $\sigma = 0,35; \; 0,525; \; 0,7$.

❖ *Characteristics of the Air Flow Passing Through the Turbine Rotor*

In the field of the turbomachinery analysis the frictional forces are evaluated with the Reynolds criteria. The values of the Reynolds number larger than $\text{Re} > 2.10^6$ are ensuring a fully turbulent flow regime. Therefore, all the investigated wind turbine operational regimes and configurations are carried out under air flow velocity, $\vartheta = 20 \; m/s$ thus ensuring fully developed turbulent flow regime.

4.3. Experimental Results Analysis

The comparison between the torque aerodynamic performance characteristics for the two, three and four-bladed Darrieus rotor configurations of the hybrid turbine with pre-set pitch angles of $\varphi = -6°$, $0°$ is presented in fig. 19.

The torque, drag force and the power coefficients are obtained through the following dependencies:

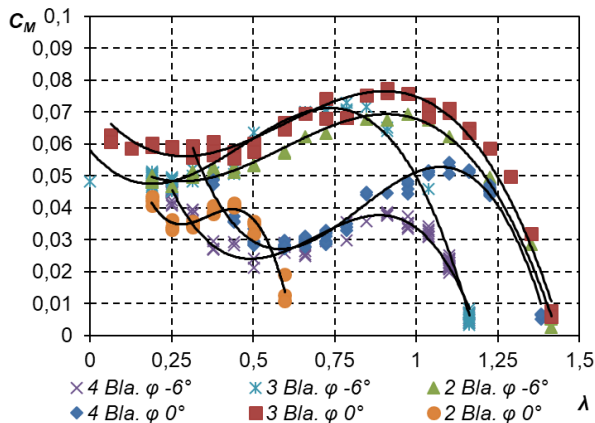$$(17) \qquad C_M = \frac{M}{\rho \vartheta^2 R^2 H},$$

$$(18) \qquad C_{FN} = \frac{F_N}{\rho \vartheta^2 R H},$$
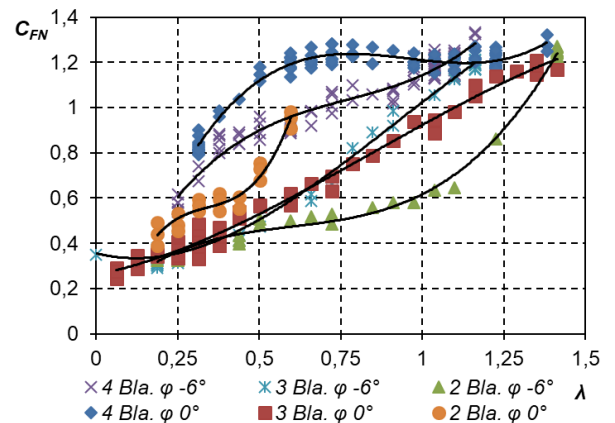
$$(19) \qquad C_P = \frac{P}{\rho \vartheta^3 R H},$$

where R is the rotor radius, H is the rotor height.

In the operational area of low TSR $\lambda < 0.5$, the predominant operational principle for all of the investigated hybrid configurations is the drag principal. The main contribution to the torque generation belongs to the Savonius rotor. After applying an approximation curve over the experimental torque coefficient results it was found out that the highest start-up coefficient $C_{M_{ST}} \approx 0.13$ belongs to the four-bladed Darrieus rotor configuration with pitch angle $\varphi = 0°$, reached zero TSR. It is a common feature for all the investigated configurations characteristics to form a col in the area of the low TSR. With the decrease of the Darrieus blade numbers the col amplitude lessens and shifts toward the lower end of the TSR area $\lambda < 0.3$. This is due to the decrease of the hybrid rotor aerodynamic drag. The lower Darrieus blades number results in decrease of the turbulent intensity, especially in the rotor upstream area. The Savonius rotor efficiency is higher under these operational conditions.

Fig. 19 Torque Aerodynamic Characteristics for Hybrid Configurations with Different Blade Numbers and Pre-set Pitch Angles

Fig. 20 Drag Force Aerodynamic Characteristics for Hybrid Configurations with Different Blade Numbers and Pre-set Pitch Angles

With the increase of the TSR $\lambda > 0.5$, the lift operational principle becomes predominant. This marks the beginning of the development of the ascending slopes of the characteristic curves. The Darrieus blade number has a significant influence on the curves slope steepness. The two-and three-bladed Darrieus variations characteristic curves have moderate ascending slopes. The maximum value of the torque coefficient, also called

nominal, belongs to the three-bladed Darrieus configuration with pitch angle of $\varphi = 0°$. The nominal value of the coefficient is $C_{M_N} = 0.077$ reached at TSR $\lambda_N = 0.91$. The three-bladed Darrieus configuration with pitch angle $\varphi = 0°$ characteristic has the wider TSR operational range $\lambda = 0.1 \div 1.1$. The relative fluctuation of the torque coefficient in this range has a value of $\psi_{CM} = 0.5$, calculated with the dependency $\psi_{CM} = \dfrac{C_{M_{max}} - C_{M_{min}}}{(C_{M_{max}} + C_{M_{min}})/2}$. The torque coefficient characteristics of the four-bladed Darrieus configuration with pitch angles of $\varphi = 0°$ and $\varphi = -6°$ have similar ascending slopes and narrow operational areas. Their torque coefficients nominal values are lower in comparison with the nominal values of the two-and three-bladed Darrieus configurations.

The differences between the characteristic curves shapes are due to the change in the hybrid turbine solidity. With the increase of the blade number the aerodynamic drag of the hybrid rotor increases. The flow passing around the rotor expands, which in its turn results in increase of the angle of attack fluctuation range $\alpha > \pm 90°$. These circumstances are contributing to the formerly occurrence of the dynamic stall phenomena and its delayed fading. The vortex structures generated and shed from the hybrid turbine comprising rotors blades are suppressing the dominance of the lift force operational principal. As a result, the span of the TSR operational area decreases. The four-bladed Darrieus configuration operates with relatively high efficiency in a narrow TSR operational area $\lambda = 0.8 \div 1.25$.

At almost all hybrid configurations the pitch angle $\varphi = -6°$ results in a decrease of the torque coefficient for the whole TSR turbine operational range. A shift in the characteristics maximums toward the area of low TSR is observed. This is explained by the additional rise in the angle of attack fluctuation range driven by the pre-set pitch angle. The negative values of the pre-set pitch angel are expected to reduce the fluctuation of the angle of attack, but values lower than $\varphi \leq -6°$ appear to be unfavourable. They are contributing to the increase of the angle of attack fluctuation range, ultimately intensifying the dynamic pulsations of pressure and velocity over the blades surfaces. The two-bladed hybrid rotor configuration with pre-set pitch angle of $\varphi = -6°$ is an exception. In this case, the pitch angle allows the turbine to reach optimal performance regime. At this configuration, the pitch angle reduces the fluctuation of the angle of attack α allowing the flow to stay attached to the blades for a larger portion through a full rotor revolution. The main factor contributing to this favourable flow-to-blade interaction is the turbine low solidity $\sigma = 0.35$. The low solidity is reducing the expansion of the flow passing around the rotor, causing a decrease in the angle of attack fluctuation range. At pitch angle $\varphi = 0°$, the generated blade lift force is not sufficient to overcome the bearing friction losses and the supporting struts aerodynamic drag, due to which the hybrid turbine is not able to reach optimal performance regime.

The torque coefficient characteristics for all the hybrid turbine configurations have steep descending slopes. This is due to the rise of the combined bearings friction losses and the aerodynamic strut and shaft drag. They are directly connected to the increase of the TSR.

A comparison between the drag force coefficient for the two, three-and four-bladed Darrieus configurations with pitch angles of $\varphi = -6°; 0°$ is shown in fig. 20. In the whole TSR operational area, the characteristic curves for all hybrid configurations have ascending trend. The rise of the drag coefficient with the increase of the TSR is due to the fall of the rotors permeability. With the fall of the permeability, the total drag of the hybrid rotor rises, causing for the larger portion of the air flow to pass around the turbine. This leads to increase of the total pressure difference in front and behind the turbine.

In the TSR area $\lambda < 0.5$, the drag coefficient for most of the hybrid configurations pitch angles has similar values. At these TSR the turbine rotational velocity is relatively low $n < 500$ min^{-1}, respectively its total drag is low and therefore the greater portion of the flow is passing through it. The differences in the drag coefficient values are due to the Darrieus rotor blades number. The higher blades number results in rising of the total aerodynamic drag, leading to higher drag loads.

With the increase of the TSR $\lambda > 0.5$, the lift operational principal becomes predominant. The Darrieus rotor rotational velocity rises, reaching peripheral velocity values higher than the airflow velocity. At this operational range of TSR, the drag coefficient is mainly affected by the rise of the hybrid rotor solidity i.e. the rise of its rotational velocity. The three-and four-blade configurations are subjected to bigger drag loads in comparison to the two-bladed configuration.

The characteristic curve which is closest to a linear trend for the whole TSR operational area belongs to the three-bladed Darrieus configuration with pitch angle of $\varphi = 0°$. Its minimum and maximum values respectively are $C_{FN\min} = 0.26$ reached at TSR $\lambda = 0.06$ and $C_{FN\max} = 1.16$ reached at TSR $\lambda = 1.4$.The drag coefficient averaged value is $C_{FN_{CP}} = 0.55$. The two-bladed configuration characteristic has a slight drop in the TSR area of around $\lambda \approx 1$, after which rises until reaching its maximum value of $C_{FN\max} = 1.27$ at $\lambda = 1.41$. Its minimum coefficient value is $C_{FN\min} = 0.25$ at TSR $\lambda = 0.18$. The average value of the coefficient in this configuration is $C_{FN_{CP}} = 0.66$.
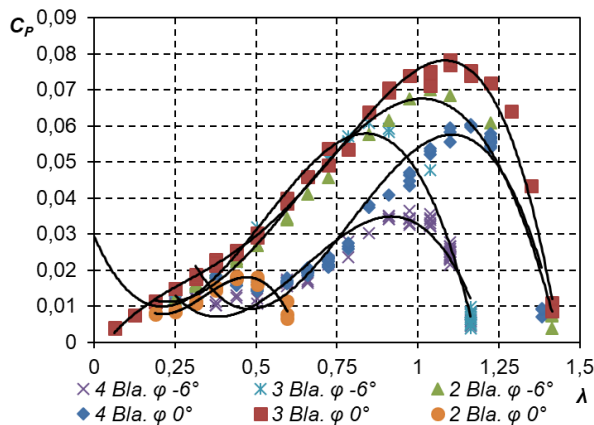
The high solidity of the four-bladed Darrieus configuration with pitch angles of $\varphi = 0°$ and $\varphi = -6°$ predetermines its higher drag coefficient values. The difference in the characteristic curves comes from the earlier flow detachment in the case of the $\varphi = -6°$ pitch angle. The earlier flow detachment is driven by the rise in the angle of attack fluctuation range i.e. the earlier dynamic stall occurrence which leads to drop in the drag coefficient average value. The drag force coefficient average value at pitch angles $\varphi = 0°$ and $\varphi = -6°$ are respectively $C_{FN_{CP}} = 1.15$ and $C_{FN_{CP}} = 1.01$.

At the two-bladed Darrieus configuration with pitch angle of $\varphi = 0°$ the maximum value of the drag coefficient is $C_{FN\max} = 1.1$ reached at TSR $\lambda = 0.65$. The operational regime at this low TSR is characterized by intensive vortex generation and shedding from the Darrieus blades. The massive vortex structures generated on the blades are briefly enlarging their pressure or suction surfaces before shedding. This leads to increase in the drag force.

The values of the pitch angle for the two, three-and four-bladed Darrieus hybrid configurations does not have any significant effect on the drag coefficient average value. The average values of the drag force coefficient in the case of the two-bladed Darrieus configuration with pitch angles of $\varphi = 0°$ and $\varphi = -6°$ are equal $C_{FN_{CP}} = 0.66$. The average values of the coefficient in the case of the three-bladed configuration with pitch angles of $\varphi = 0°$ and $\varphi = -6°$ are respectively $C_{FN_{CP}} = 0.54$ and $C_{FN_{CP}} = 0.55$. The average values of the coefficient in the case of the four-bladed configuration with pitch angles of $\varphi = 0°$ and $\varphi = -6°$ are respectively $C_{FN_{CP}} = 1.15$ and $C_{FN_{CP}} = 1.01$. The pre-set pitch angle values are affecting the drag coefficient performance curve shape. The decrease of the pitch angle to the value of $\varphi = -6°$ is leading to increase of the angle of attack. This results in early dynamic stall occurrence, which is especially pronounced in the case of the four-bladed turbine configuration. This ultimately results in drop of the drag coefficient through the whole turbine TSR operational range.

The effect of the pre-set pitch angle reduction to $\varphi = -6°$ over the two-bladed hybrid configuration is a reduction in the dynamic stall intensity. The blades surface area does not undergo any significant alterations due to the formation and development of vortex structures. Therefore, the rise of the drag coefficient value is driven by the increase of the rotor RPM i.e. the increase of the solidity.

A comparison between the output power coefficient for the two, three-and four-bladed Darrieus configurations with pitch angles of $\varphi = -6°; 0°$ is shown in fig. 21. The characteristic curves for all the investigated hybrid turbine configuration have similar shapes – a clearly formed maximum with steep ascending and descending slopes. The blade numbers have significant effect on the hybrid turbine performance. The increase of the blades results in rising of the turbulent intensity, therefore to the generation of large vortex structures. The vortex structures are interacting with the turbine blades in the rotor downstream area. This reduces the energy extraction efficiency in this area. The increase of the turbine solidity results in rising of the total hydrodynamic losses. Due to the high rotor solidity, the flow passing around the turbine is expanding due to the decrease of the air flow velocity drop through the rotor swept area. This contributes to the increase of the angle of attack fluctuation range according to equation (2.4). These operational conditions are ultimately leading to significant rise in the dynamic stall intensity. Due to the broad angle of attack fluctuation range, the flow is detaching and reattaching to the turbine blades multiple time during the course of a single rotor revolution.
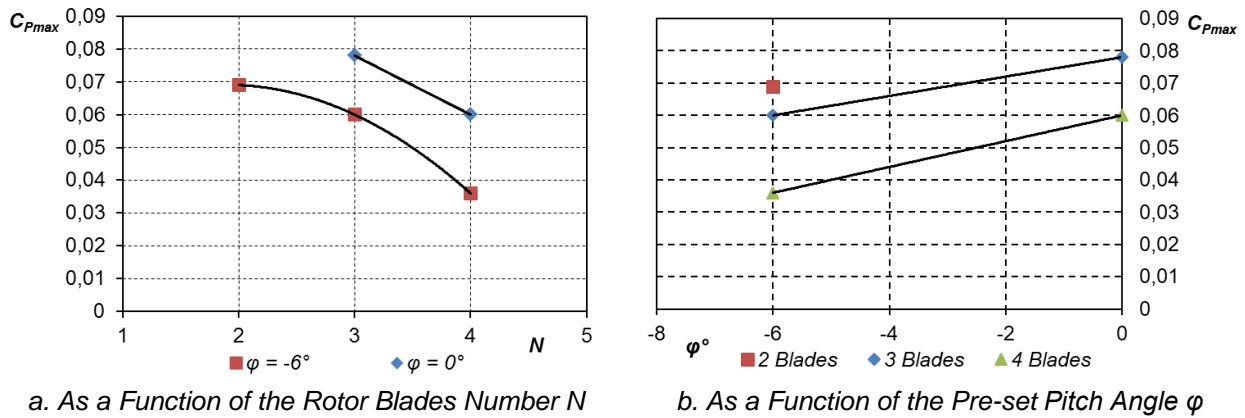

Fig. 21 Output Power Aerodynamic Characteristics of Hybrid Configurations with Different Blade Numbers and Pre-set Pitch Angles

The turbine solidity affects the output power coefficient maximum value and its corresponding TSR. The hybrid rotor configurations with low solidity ($\sigma \leq 0.525$) are performing effectively in the range of the high TSR values ($\lambda > 1$). Their performance curves have moderate ascending and descending slopes. The configurations with high solidity rotors perform effectively in the range of the low TSR values. Their performance curves have steep ascending and descending slopes, which are forming a narrow operating area of TSR. The maximums of the output power coefficient curves are called nominal output power coefficient performance points. With the decrees of the blades number, the value of the power coefficient rises, and its location moves towards the area of the high TSR values. The maximum value of the nominal performance point belongs to the three-bladed Darrieus hybrid configuration with pre-set pitch angle $\varphi = 0°$. The nominal value of the power coefficient at this configuration is $C_{P_N} = 0.078$ reached at nominal TSR of $\lambda_N = 1.1$.
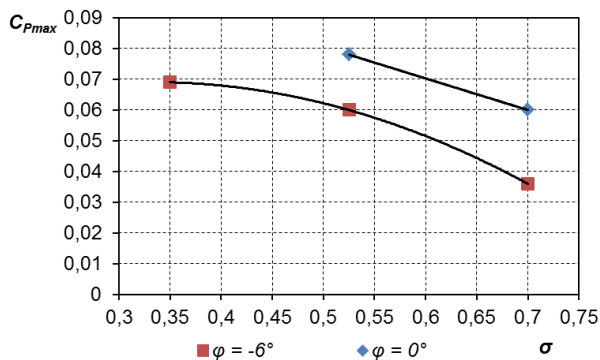
The power coefficient maximum value rate of change as a function of the hybrid turbine blades number and pre-set pitch angles is depicted in fig. 22. As can be seen from fig. 22 a, with the decrees of the blades number the maximum value of the power coefficient rises, reaching its peak of $C_{P_{max}} = 0.078$ for the three-bladed Darrieus configuration with pitch angle of $\varphi = 0°$. The rise of the power coefficient with the reduction of the blades number is due to the decrease of the turbine aerodynamic drag. The lower aerodynamic drag results in increase of the rotor permeability which ultimately yields in reduced expansion of the flow passing around the turbine. Those operational conditions are contributing to the reduction in the angle of attack fluctuation range. The narrow-angle of attack range of change is prolonging the time during which the flow stays attached to the

blades at the course of a full rotor revolution. The intensity of the vortex generation, development and detachment are reduced i.e. the influence of the dynamic stall phenomena is less pronounced. The result of those performance conditions is reduction of the turbine vortex driven hydraulic losses and substantial rise of the hybrid rotor energy conversion throughout both upstream and downstream turbine areas.

a. As a Function of the Rotor Blades Number N

b. As a Function of the Pre-set Pitch Angle φ

Fig. 22 Maximum Power Coefficient Performance Characteristics

The influence of the pre-set pitch angle over the maximum values of the power coefficient is shown in fig. 22 b. The power coefficient reaches higher values at pre-set pitch angle of $\varphi = 0°$ in comparison with the pitch angle of $\varphi = -6°$, regardless of the rotor blades number. The two-bladed Darrieus configuration with pitch angle $\varphi = 0°$ stands out as an exception due to its inability to reach optimal performance regime. In this configuration, the angle of attack is fluctuating in a range in which the lift force acting on the blades has low values. Due to this circumstance, the turbine is not able to overcome the friction losses in the bearings and the aerodynamic drag of the supporting struts, shaft etc. The pre-set pitch angle $\varphi = -6°$ introduces an initial change in the angle of attack diapason yielding an increase of the dynamic stall effect over the turbine performance. The intensified vortex generation, development and shedding from the rotor blades is increasing the hydraulic losses and reducing the energy extraction of the hybrid turbine throughout all of its swept area.

Fig. 23 Maximum Power Coefficient Performance Characteristic as a Function of the Rotor Solidity σ

The two-bladed Darrieus configuration with pitch angle of $\varphi = -6°$ performance also stands out as an exception. At this configuration, the pre-set pitch angle $\varphi = -6°$ is allowing the turbine to reach optimal performance operational regime. At this configuration, the combination of the high rotor permeability and pitch angle $\varphi = -6°$ is resulting in favourable angle of attack fluctuation diapason. The values of the generated lift force are sufficient to overcome the combined energy losses and are allow the turbine to reach optimal performance operational regime. The data presented in fig. 22 allow us to conclude that the optimal hybrid turbine configuration is the three-bladed Darrieus variation with pre-set pitch angle of $\varphi = 0°$.
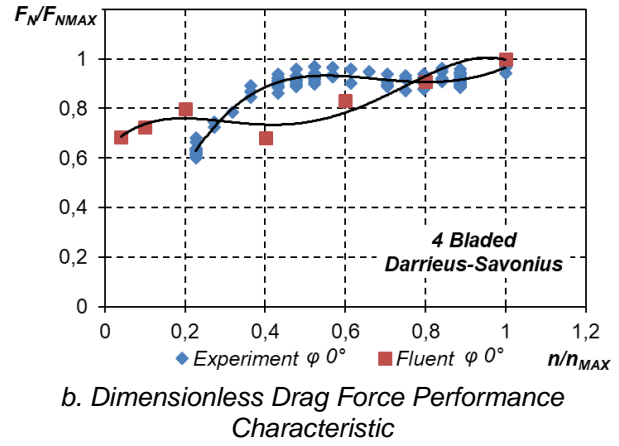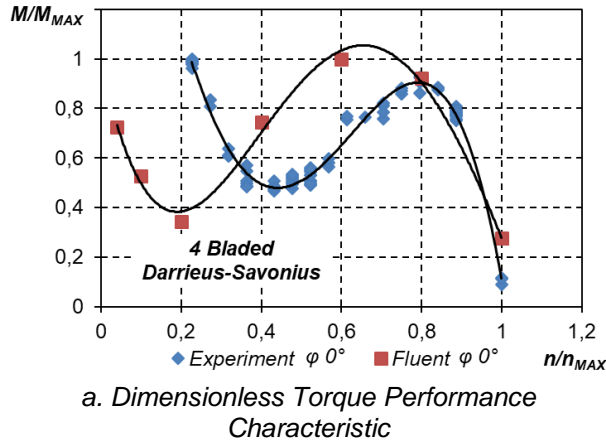
The rate of change in the maximum value of the power coefficient as a function of the rotor solidity at pre-set pitch angles of $\varphi = 0°$ and $\varphi = -6°$ is presented in fig. 23. As can be

seen from the chart the maximum value of the power coefficient drops with the increase of the solidity. The maximum coefficient value is affected by the Darrieus rotor blades pitch angle. The higher maximum values are reached at pre-set pitch angle of $\varphi = 0°$. The difference between the power coefficient maximum values for the two pitch angles is diminishing with the decrease of the rotor solidity. This is explained by the reduction of the hybrid rotor total aerodynamic drag due to the decrease in the angle of attack fluctuation range.
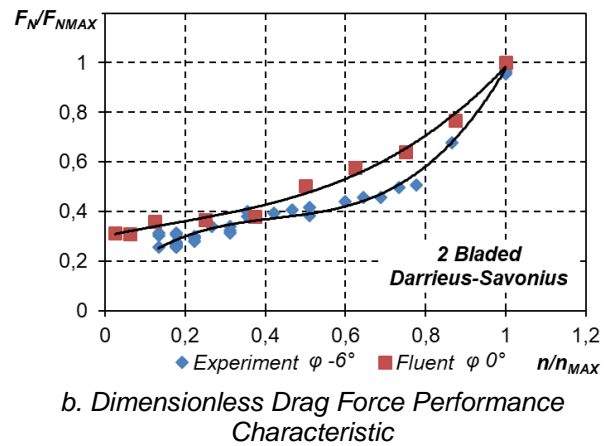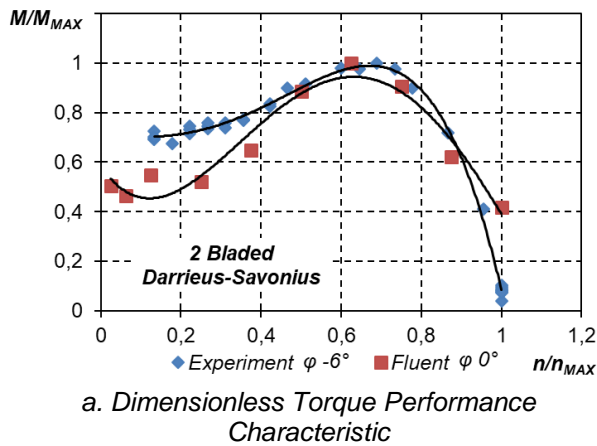
4.4. Comparison Between the Theoretical and Experimental Results

Comparison between the dimensionless performance theoretical and experimental characteristics regarding the maximum values of the torque, drag and the output power for the two-and three-bladed Darrieus configurations are presented on fig. 24, fig. 25 and fig. 26. As can be seen from the charts the theoretical model replicates well the experimental performance curves. The discrepancies between the experimental and the theoretical curves are explained by the fact that the experimental study is carried over a hybrid configuration with a two-staged Savonius comprising rotor. Wears the assumption for a 2D theoretical modelling limits the investigation to a single-staged (2D geometrical model) Savonius comprising rotor. The two-staged Savonius rotor gives better start-up characteristics to the hybrid turbine but introduces additional drag which leads to drop in the turbine energy extraction. This effect is most strongly pronounced in the four-bladed Darrieus configuration. At this configuration, the Savonius comprising rotor is contributing to the increase of the solidity effect over the hybrid turbine operation. The lower range of RPM at which the experimental characteristics are developing is explained by the inability of the hybrid turbine to overcome the mechanical friction losses in the bearings, the hydraulic losses produced by the supporting struts, the shaft and all the supporting elements. The total aerodynamic losses increase with the rise of the hybrid rotor solidity. The high solidity of the four-bladed Darrieus rotor configuration ($\sigma = 0.7$) determines its high total aerodynamic drag due to which the major portion of the airflow is passing around the hybrid turbine.
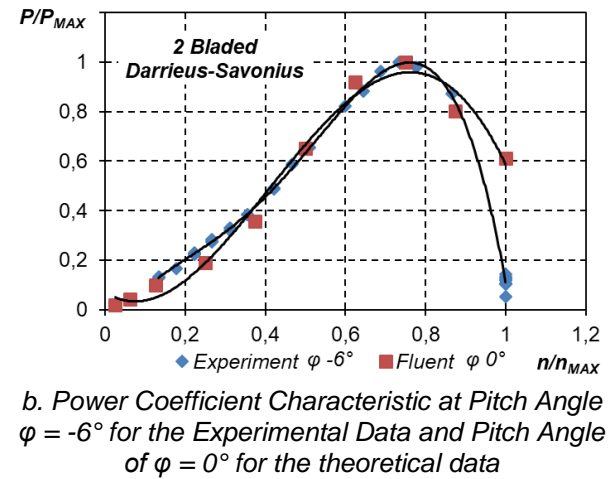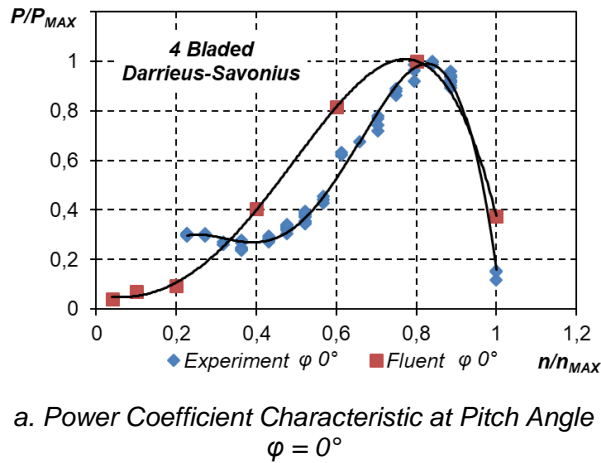
The theoretical results regarding the values of the torque and the drag force are overestimating the experimentally obtained values. For both hybrid turbine configurations (two-bladed and three-bladed Darrieus) the overestimation of the experimentally obtained values is explained by the made simplifying assumptions regarding the 2D URANS modelling approach. The highest impact on the performance prediction values belongs to the assumption for a two-dimensional flow. In the case of a real flow development, the vortex structures generation and expansion over a blade surface are spreading in all directions (in three-dimensional space). In the case of 2D numerical modelling the vortex structures development is confined in a 2D plane. This results in the development of large homogenous structures. Another major drawback of the URANS modelling approach is its time averaging operational principle. The Reynolds stress tensors transported as turbulent pulsations are not calculated but modelled through time averaging. The main drawback of the 2D URANS approach is the modelling of periodically shedding large homogenous vortex structures. The discrepancy between the theoretical and experimental results is explained by the generation of large vortex structures on the blades surfaces. Those structures are briefly enlarging the blades surface areas before shedding. This results in change of the airfoil coefficients, therefore to overestimation of the theoretical lift and drag forces. This effect is most strongly pronounced at the low TSR turbine operational regimes which are characterized by a higher rate of the angle of attack fluctuations. At these operational conditions, the dynamic stall phenomena are predominant – periodical formation and detachment of large vortex structures. An additional factor, contributing to the overestimation of the theoretical torque and power coefficients (fig. 26) is the neglect of the blade edges vortex generation in the case of finite span blades.

a. Dimensionless Torque Performance
Characteristic

b. Dimensionless Drag Force Performance
Characteristic

**Fig. 24 Dimensionless Performance Characteristics of the Four-Bladed Darrieus Hybrid Turbine
Configuration with Pitch Angle of φ = 0°**

a. Dimensionless Torque Performance
Characteristic

b. Dimensionless Drag Force Performance
Characteristic

**Fig. 25 Dimensionless Performance Characteristics of the Two-Bladed Darrieus Hybrid Turbine
Configuration with Pitch Angle of φ = -6° for the experimental data and Pitch Angle of φ = 0° for
the theoretical data**

a. Power Coefficient Characteristic at Pitch Angle
φ = 0°

b. Power Coefficient Characteristic at Pitch Angle
φ = -6° for the Experimental Data and Pitch Angle
of φ = 0° for the theoretical data

**Fig. 26 Dimensionless Performance Characteristics of the Two-and Four-Bladed Darrieus Hybrid
Configurations**

In the case of the two-dimensional Darrieus hybrid configuration, the experimental data regarding the $\varphi = -6°$ pitch angle is compared to the theoretical data regarding the $\varphi = 0°$ pitch angle. During the conduction of the experimental investigation over the two-bladed Darrieus hybrid configuration with pitch angle of $\varphi = 0°$ the turbine was not able to overcome the frictional losses in the bearings and the additional aerodynamic losses produced by the supporting struts, shaft etc. As a result, the hybrid turbine is not able to

reach optimal performance operational regime. Due to which the theoretical data regarding the $\varphi = 0°$ pitch angle is compared to the experimental data regarding the pitch angle of $\varphi = -6°$.

5. CHAPTER CONCLUSIONS

5.1. Conclusions and Recommendations

1. The theoretical results independence study regarding the modelling of the number of full Darrieus and Savonius rotors revolutions showed that periodicity in the solution is achieved after the fifth revolution.

2. After analysing the computational mesh quality data, it was proven that the value of the near wall criteria *y+*, ensuring the modelling of the laminar boundary sublayer is $y^+ < 5$.

3. The 2D URANS modelling approach tends to overestimate the theoretical hybrid turbine torque and power coefficients, especially in high angles of attack flow conditions. Besides that, the modelling approach replicates well the shapes of the experimental performance curves.

4. It was found out that the two-dimensional simulation successfully models the complex vortex structures generation, development and detachment from the blades surfaces. The theoretical investigation showed that at low TSR operational regimes the dynamic stall phenomena is predominant. Wears at high TSR operational regimes the intensity of the vortex generation drops, the velocity of the flow passing through the rotor also diminishes. This results in reduction of the local blades angle of attack fluctuation range, ultimately yielding in decrease of the lift force values.

5. It was found out that the 2D URANS approach lacks the ability to model the vortex structures interactions and dissipation in greater detail. The 2.5D LES approach has the upper hand regarding the physical accuracy of the large vortex structures interaction and dissipation modelling.

6. The major shortcomings of the 2.5D LES modelling approach are the high demands towards the computational hardware and the long computational time. Each of the carried 2D URANS simulations took up to $26 \div 28$ computational hours, plus the simulation preparation time and the time needed for extraction and postprocessing the numerical data. Each of the 2.5D LES simulations took up to 384 computational hours (16 days), plus the time for simulation preparation and the time needed for extraction and postprocessing the computational data.

7. It was proven theoretically and experimentally that the hybrid turbine configurations with low solidity σ reach high efficiently at high TSR operational regimes. On the other hand, the hybrid configurations with high solidity σ reach high efficiency at low TSR operational regimes.

8. Theoretically, it was found out that the increase of the hybrid turbine blades number and the rotor solidity leads to rising in the vortex generation, development and shedding intensity. The rise in the turbulent structures interference with the turbine blades, especially in the downstream rotor area results in increase of the total turbine aerodynamic loss. The flow passing around the rotor expands the angle of attack pulsation range broadens and the values of the drag force rise.

9. Experimentally it was found out that increase of the Darrieus rotor blade numbers improves its self-starting capabilities, but reduces the maximum value of the power coefficient $C_{P\max}$.

10. Experimentally it was proven that the three-bladed Darrieus hybrid configuration has the best self-starting capabilities and reaches higher efficiency values in comparison with the two-and four-bladed configurations. The experimentally obtained maximum performance operational regime regarding the optimal hybrid turbine configuration has maximum power coefficient of $C_{P\max} \approx 0.078$ reached at nominal TSR of $\lambda_{H} \approx 1.1$.

11. It was experimentally proven that the hybrid configurations with pre-set pitch angles of $\varphi = \pm 16°$ exhibits tendency to start revolving clockwise, whereas the design rotational direction is counter clockwise. Therefore, investigation of blade pre-set bitch angles beyond the diapason of $\varphi = \pm 16°$ is not recommended.

12. Experimentally it was found out that the pre-set pitch angle has strong effect over the investigated turbine configurations performance curves shape and the position of their maximums. Therefore, the pre-set pitch angel can be used as turbine power regulation mechanism.

5.2. Academically - Applicable Contributions

1. It was proven that the hybrid rotor solidity σ strongly affects the maximum value of the power coefficient $C_{P\max}$. With the increase of σ, the power coefficient $C_{P\max}$ drop can be approximated with linear law.

2. It was found out that the pre-set pitch angle φ has a strong effect on the power coefficient maximum values. Pitch angle values differing from $\varphi = 0°$ are leading to drop of the power coefficient which can be approximated by a linear law.

3. During the conduction of the experimental investigation over the hybrid turbine configurations with pre-set pitch angles of $\varphi = -16°$; $6°$; $16°$ the wind, rotors exhibit a brief tendency of clockwise (opposite to design direction) direction rotation. This tendency is easily overcome by the high start-up torque generated by the Savonius rotor.

4. The recommended values regarding the hybrid turbine geometrical parameters are established – solidity $\sigma \le 0.525$, pre-set pitch angle $\varphi = 0°$, rotor radius $R = 0.2\ m$ and blades number $N = 3$. These parameters ensure the operation of the hybrid turbine with high value of the power coefficient $C_{P\max}$.

5. The optimal TSR operational regimes for the hybrid turbine are established. In order to operate effectively with high values of the power coefficient the recommended TSR operational range is $\lambda \ge 1$.

6. The optima geometrical configuration of the investigated hybrid wind turbine Darrieus-Savonius is established. The optimal configuration includes blade number $N = 3$; pre-set pitch angle $\varphi = 0°$; Darrieus rotor radius $R_{D} = 0.2\ m$; Darrieus rotor blade height $H_{D} = 0.4\ m$; comprising rotors (Darrieus and Savonius) diameters ratio $D_{S} / D_{D} = 0.25$; comprising rotors height ratio $H_{S} / H_{D} = 0.25$.

5.3. Applicable Contributions

1. A methodology for experimental investigation of vertical axis wind turbines was developed. Based on the developed methodology, an automated test bench was constructed. The test bench can also be used for horizontal axis wind turbines investigations. Furthermore, laboratory experimental-investigation classes can be conducted as a part of the university engineering curriculum.

2. The numerical parameters at which a solution independence regarding the 2D and 2.5D simulations is achieved are established. The minimum number of the modelled full turbine revolutions is five. To ensure an adequate laminar boundary sublayer modelling, the near wall criteria value must be lower than $y^+ < 5$.

DOCTORAL THESIS LIST OF PAPERS

1. Ahmedov A., Tujarov Kr., Popov G., Jeleva I., Nikolaev I., Klimentov K. Theoretical Models for the Investigation of Wind Turbines with Vertical Axis of Rotation, Type Darrieus - Momentum models. Mechanics of the Machines, Varna 2013, issue 2, p. 27-32, ISSN 0861-9727.

2. Ahmedov A., Tujarov Kr., Popov G., Jeleva I., Nikolaev I., Klimentov K. Vortex and Cascade Models for the Investigation of Wind Turbines with Vertical Axis of Rotation - Type Darrieus. Proceedings volume 51, book 1.2, Heat transfer, hydraulic and pneumatic engineering. Ecology and environmental protection. Design and ergonomics, Ruse 2012, page 154-159, ISBN 1311-3321.

3. Ahmedov A., Tujarov Kr., Popov G. Methodology for Numerical Modelling the Performance of Vertical Axis Wind Turbines. In: University of Ruse Proceedings volume 53, book 1.2, Heat transfer, hydraulic and pneumatic engineering. Ecology and environmental protection. Design and ergonomics, Ruse 2014, ISBN 1311-3321.

4. Ahmedov A. Methodology for Experimental Study of Wind Turbines with Vertical Axis of Rotation. Proceedings volume 52, book 1.2, Heat transfer, hydraulic and pneumatic engineering. Ecology and environmental protection. Design and ergonomics, Ruse 2013, ISBN 1311-3321.

5. Ahmed Ahmedov and K. M. Ebrahimi, "Numerical Modelling of an H-type Darrieus Wind Turbine Performance under Turbulent Wind". American Journal of Energy Research, vol. 5, no. 3 (2017): 63-78. doi: 10.12691/ajer-5-3-1.

GRATITUDE